AD-A134 723   VALIDATION OF THE CONTRAST ATTENUATION TECHNIQUE (CAT)   1/2
              FOR DEDUCING DUST.. (U) TELEDYNE BROWN ENGINEERING
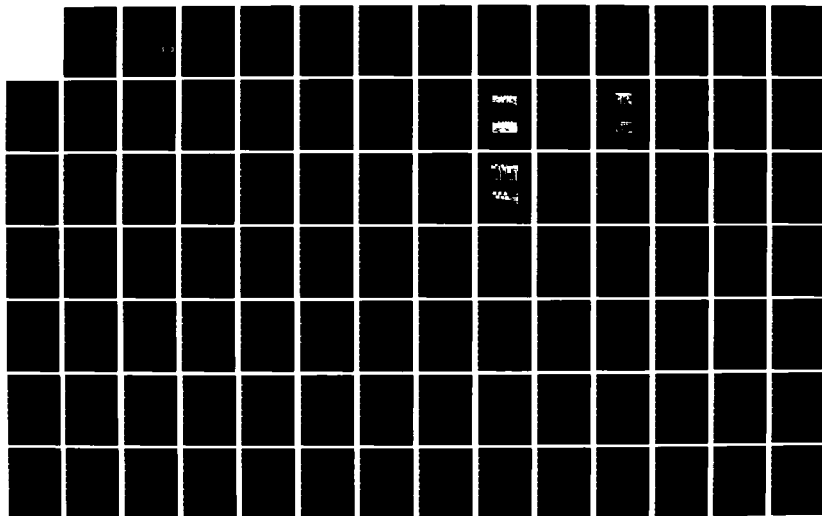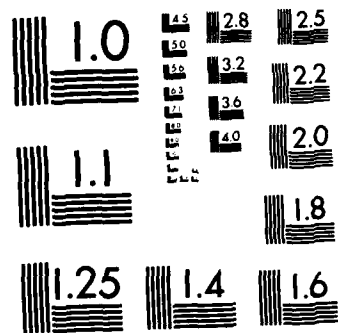   HUNTSVILLE AL   M L PRICE 28 FEB 82 SD81-DNA2574
UNCLASSIFIED DNA-TR-81-81 DNA001-81-C-0129   F/G 14/5   NL

MICROCOPY RESOLUTION TEST CHART
NATIONAL BUREAU OF STANDARDS-1963-A

DNA-TR-81-81

VALIDATION OF THE CONTRAST ATTENUATION TECHNIQUE (CAT) FOR DEDUCING DUST DENSITIES FROM PHOTOGRAPHIC RECORDS TAKEN DURING THE MILL RACE HIGH EXPLOSIVE TEST

Melvin L. Price
Teledyne Brown Engineering
Cummings Research Park
Huntsville, Alabama 35807

28 February 1982

Technical Report

CONTRACT No. DNA 001-81-C-0129

DTIC
ELECTE
NOV 15 1983
S
B

DTIC FILE COPY

Prepared for
    Director
    DEFENSE NUCLEAR AGENCY
    Washington, DC 20305

83   010

REPORT DOCUMENTATION PAGE		READ INSTRUCTIONS BEFORE COMPLETING FORM
1. REPORT NUMBER DNA-TR-81-81	**2. GOVT ACCESSION NO.** AD-A134 723	**3. RECIPIENT'S CATALOG NUMBER**
4. TITLE (and Subtitle) VALIDATION OF THE CONTRAST ATTENUATION TECHNIQUE (CAT) FOR DEDUCING DUST DENSITIES FROM PHOTOGRAPHIC RECORDS TAKEN DURING THE MILL RACE HIGH EXPLOSIVE TEST		**5. TYPE OF REPORT & PERIOD COVERED** Technical Report
		6. PERFORMING ORG. REPORT NUMBER SD81-DNA-2574
7. AUTHOR(s) Melvin L. Price		**8. CONTRACT OR GRANT NUMBER(s)** DNA 001-81-C-0129
9. PERFORMING ORGANIZATION NAME AND ADDRESS Teledyne Brown Engineering Cummings Research Park Huntsville, Alabama 35807		**10. PROGRAM ELEMENT, PROJECT, TASK AREA & WORK UNIT NUMBERS** Task N99QAXAG-00001
11. CONTROLLING OFFICE NAME AND ADDRESS Director Defense Nuclear Agency Washington, D.C. 20305		**12. REPORT DATE** 28 February 1982
		13. NUMBER OF PAGES 96
14. MONITORING AGENCY NAME & ADDRESS(If different from Controlling Office)		**15. SECURITY CLASS. (of this report)** UNCLASSIFIED
		15a. DECLASSIFICATION/DOWNGRADING SCHEDULE N/A since UNCLASSIFIED

16. DISTRIBUTION STATEMENT (of this Report)

Approved for public release; distribution unlimited.

17. DISTRIBUTION STATEMENT (of the abstract entered in Block 20, if different from Report)

18. SUPPLEMENTARY NOTES

This work was sponsored by the Defense Nuclear Agency under RDT&E RMSS Code B342081466 N99QAXAG00001 H2590D.

19. KEY WORDS (Continue on reverse side if necessary and identify by block number)

Dust Concentration	Nuclear Sweep-up Dust	Scattering
Dust Density	High Explosive Test	Visual Range Validation
Dust Particle size distribution	MILL RACE	Densitometry
Dust Extinction Coefficient	Visibility	Contrast Measurements
Shock-Entrained Dust	Contrast Attenuation Technique	Extinction

20. ABSTRACT (Continue on reverse side if necessary and identify by block number) The MILL RACE high explosive test was used to validate the Contrast Attenuation Technique for deducing dust densities by measuring the reduction in contrast between an object and its background. A total of six movie cameras were placed at the 10 psi and 20 psi distance from GZ along with six photo targets at each location. Movies were obtained from just before the detonation to up to 5 minutes after and showed passage of the dust cloud as it enveloped the cameras and targets until the air was essentially free from dust. The films were processed according to standard techniques and the resulting data analyzed on both a diffuse and microdensitometer. Application of

DD , FORM JAN 73 **1473** EDITION OF 1 NOV 65 IS OBSOLETE

20. ABSTRACT (Continued)

the Contrast Attenuation Technique produced a set of dust density vs time data which were compared with sampled measurements taken at MILL RACE in the same location and at the same time. The results showed agreement to a factor of 2.4 ± 0.61 over 60 seconds of data.

PREFACE

Accession For	
NTIS GRA&I	✔
DTIC TAB	[]
Unannounced	[]
Justification	
By	
Distribution /	
Availability Codes	
Dist	Avail and/or Special
A-1	

1

TABLE OF CONTENTS

LIST OF ILLUSTRATIONS

LIST OF TABLES

Conversion factors for U.S. customary to metric (SI) units of measurement.

To Convert From	To	Multiply By
angstrom	meters (m)	1.000 000 X E -10
atmosphere (normal)	kilo pascal (kPa)	1.013 25 X E +2
bar	kilo pascal (kPa)	1.000 000 X E +2
barn	meter^2 (m^2)	1.000 000 X E -28
British thermal unit (thermochemical)	joule (J)	1.054 350 X E +3
cal (thermochemical)/cm^2§	mega joule/m^2 (MJ/m^2)	4.184 000 X E -2
calorie (thermochemical)§	joule (J)	4.184 000
calorie (thermochemical)/g§	joule per kilogram (J/kg)*	4.184 000 X E +3
curie§	giga becquerel (GBq)‡	3.700 000 X E +1
degree Celsius‡	degree kelvin (K)	$t_K = t°_C + 273.15$
degree (angle)	radian (rad)	1.745 329 X E -2
degree Fahrenheit	degree kelvin (K)	$t_K = (t°_F + 459.67)/1.8$
electron volt§	joule (J)	1.602 19 X E -19
erg§	joule (J)	1.000 000 X E -7
erg/second	watt (W)	1.000 000 X E -7
foot	meter (m)	3.048 000 X E -1
foot-pound-force	joule (J)	1.355 818
gallon (U.S. liquid)	meter^3 (m^3)	3.785 412 X E -3
inch	meter (m)	2.540 000 X E -2
jerk	joule (J)	1.000 000 X E +9
joule/kilogram (J/kg) (radiation dose absorbed)§	gray (Gy)*	1.000 000
kilotons§	terajoules	4.183
kip (1000 lbf)	newton (N)	4.448 222 X E +3
kip/inch^2 (ksi)	kilo pascal (kPa)	6.894 757 X E +3
ktap	newton-second/m^2 (N-s/m^2)	1.000 000 X E +2
micron	meter (m)	1.000 000 X E -6
mil	meter (m)	2.540 000 X E -5
mile (international)	meter (m)	1.609 344 X E +3
ounce	kilogram (kg)	2.834 952 X E -2
pound-force (lbf avoirdupois)	newton (N)	4.448 222
pound-force inch	newton-meter (N·m)	1.129 848 X E -1
pound-force/inch	newton/meter (N/m)	1.751 268 X E +2
pound-force/foot^2	kilo pascal (kPa)	4.788 026 X E -2
pound-force/inch^2 (psi)	kilo pascal (kPa)	6.894 757
pound-mass (lbm avoirdupois)	kilogram (kg)	4.535 924 X E -1
pound-mass-foot^2 (moment of inertia)	kilogram-meter^2 (kg·m^2)	4.214 011 X E -2
pound-mass/foot^3	kilogram-meter^3 (kg/m^3)	1.601 846 X E +1
rad (radiation dose absorbed)§	gray (Gy)*	1.000 000 X E -2
roentgens§	coulomb/kilogram (C/kg)	2.579 760 X E -4
shake	second (s)	1.000 000 X E -8
slug	kilogram (kg)	1.459 390 X E +1
torr (mm Hg, 0° C)	kilo pascal (kPa)	1.333 22 X E -1

*The gray (Gy) is the accepted SI unit equivalent to the energy imparted by ionizing radiation to a mass of energy corresponding to one joule/kilogram.
†The becquerel (Bq) is the SI unit of radioactivity; 1 Bq = 1 event/s.
‡Temperature may be reported in degree Celsius as well as degree kelvin.
§These units should not be converted in DNA technical reports; however, a parenthetical conversion is permitted at the author's discretion.

6

SECTION 1

INTRODUCTION AND BACKGROUND

1.1   INTRODUCTION

The MILL RACE High Explosive Test was conducted on September 16, 1981, at White Sands Missile Range, New Mexico. Sponsored by Field Command of the Defense Nuclear Agency, it consisted of a number of experiments and/or engineering tests by both Government Agencies and private contractors. Teledyne Brown Engineering (TBE) was prime contractor for the Contrast Attenuation Technique (CAT) experiment which is the subject of this Report.

Previous work by TBE under DNA sponsorship led to the development of the CAT to deduce dust densities from photographic films. The objective of the MILL RACE experiment was primarily to validate the CAT methodology which could then be used to obtain quantitative estimates of dust densities produced during nuclear weapons testing at the Nevada Test Site (NTS). It was not the intent of the MILL RACE CAT test to obtain and use the data for scaling from non-nuclear to nuclear cases.

Because of a number of questions concerning the absolute accuracy of the CAT in deducing dust densities from NTS films, this test was designed to reproduce as closely as possible the experimental apparatus and physical conditions found for many of the NTS tests in a carefully controlled and specified parametric manner. Data obtained from this experiment would be used to determine both the accuracy and sensitivity of the CAT and thus, hopefully, provide DNA and its contractors with a reliable method for using the NTS film data to support current phenomenology studies.

Figure (1-1) depicts one of two similar test stations fielded by TBE for the MILL RACE Test. The two camera enclosures contained a total of three cameras—two in the enclosure nearest GZ and one in the other enclosure. All three cameras had fields of view containing all of the targets; the camera nearest GZ (camera A) was used as the reference line of sight so that the six targets were symmetrically spaced within its field of view. The six targets were designed to provide equal angular dimensions when viewed by camera A of approximately 4° x 4°, with adequate spacing between targets to measure the adjoining background radiance.

Also shown in Figure 1-1 are several dust sampling and measuring instruments. Although not part of the TBE-fielded equipment, these
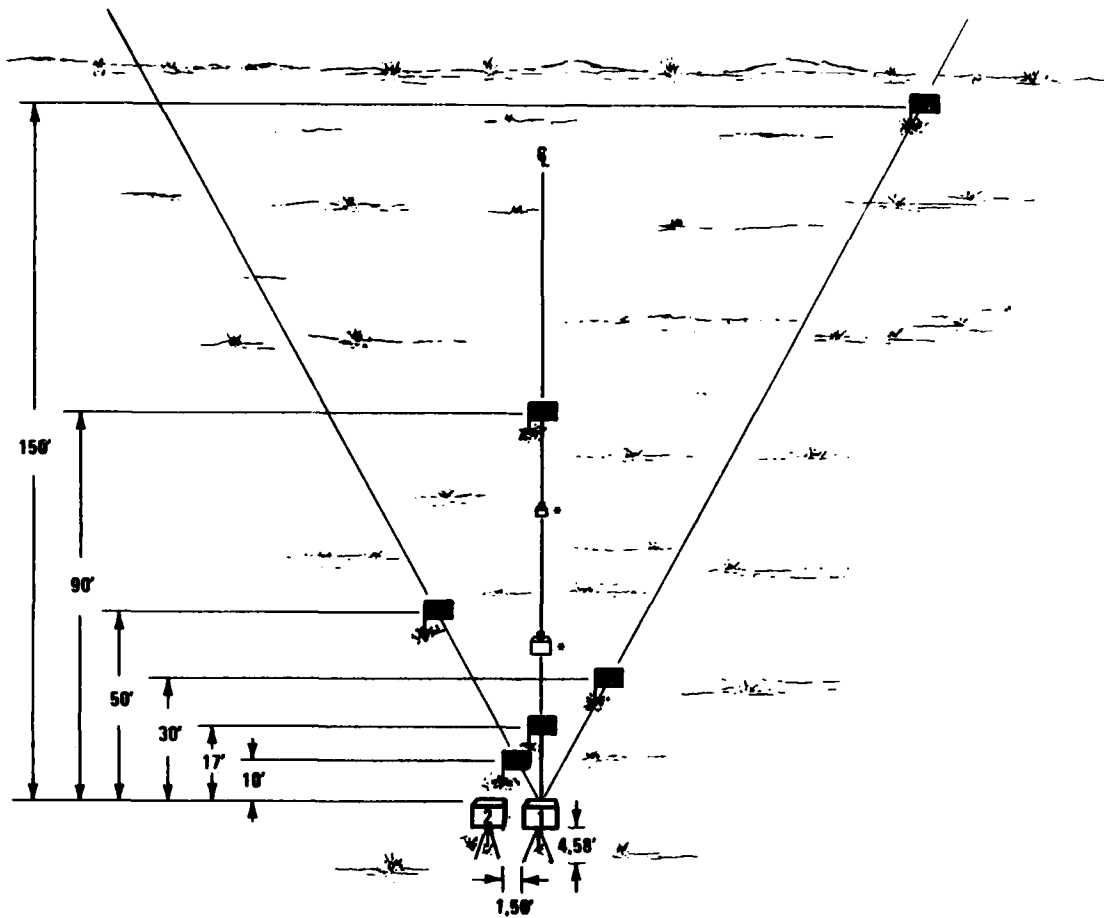
Fig.(1-1) Layout of the CAT validation experiment at MILL RACE. Shown are two camera enclosures (labeled 1 and 2) and six photo-targets. Camera enclosure 1 contained two cameras—a GSAP nearest GZ and a Flight Research. The optical centerline passed through the GSAP camera and through the center of the photo-targets located at 17' and 90'. The two units denoted with asterisks on the center were PMS dust sampling and measurement instruments used for real time dust density and particle size distribution determination.

measurements were conducted by SAI as an integral component of the total validation of the CAT. In addition, at the station nearest GZ (´20 psi), SRII fielded a microwave transmission experiment within the field of view of our cameras to obtain attenuation vs dust density data during MILL RACE; this also was part of the CAT validation experiment.

Two test stations were fielded to insure that sufficient dust would be generated at one or both sites for the CAT validation test. Selection of the two locations was governed by several considerations: first, the validation experiment was predicated on obtaining a large enough dust cloud to encompass the cameras, targets and all of the surrounding area and at a high enough density to cause total obscuration of targets as close as ten feet from the cameras; second, the experiment had to survive the effects of the detonation and continue to operate thereafter. After studying data from several previous H. E. tests, it became clear that a site at 20 psi would satisfy the first requirement while allowing us to meet the second requirement with reasonable confidence. Because we were not absolutely convinced that survival was guaranteed at 20 psi, we decided to place a second test station at 10 psi which was far enough away from GZ to guarantee survival but not clearly within the heavy dust cloud as predicted from previous tests. It turned out that usable data was obtained from both stations although the 20 psi station suffered some damage, albeit not irreparable as far as validating the CAT.

1.2   BACKGROUND

Nuclear produced dust has stymied the best efforts of many researchers to accurately predict its formation, motion, intensity and dispersion under various conditions of yield, height-of-burst, surface conditions, etc. For many military systems, both tactical and strategic, the presence of large dust concentrations can severly degrade the performance of radar, IR sensors, missiles, etc. Recently there has been a fairly substantial renewed effort to build computer models that accurately predict the dust environment produced during nuclear exchanges. Unfortunately, there are no ways to test these models under realistic conditions, i.e., an atmospheric nuclear test. Lven the use of high explosive tests has been criticized as not simulating a nuclear explosion as far as the dust environment is concerned. On the other hand, there presently exists a large data base from the atmospheric test program dating back to the 1950s. Much of these data were recorded on photographic films and consist of, typically, some object being photographed while exposed to the effects of an atmospheric nuclear burst. For many of the films, the data include the shock-entrained dust (also known as sweep-up dust) that was generated outside of the crater by the passage over the ground of the shock wave. If one could analyze this dust versus time data and extract quantitative dust densities, then the resulting information would be very useful in testing different computer models under different burst conditions.

The Contrast Attenuation Technique (CAT) for deducing dust density from photographic film was developed to use in analyzing existing films (Reference 1). Results have been very encouraging and a considerable amount of data have been and continue to be extracted from the extensive nuclear test film library. The purpose of the MILL RACE validation experiment of the CAT methodology was to reduce the uncertainties in using these data by demonstrating in a simple, carefully controlled test, the sensitivity of the various elements used in the CAT.

1.   "Determination of Shock-Entrained Dust Concentration from Photographic Records of Nuclear Weapon Tests," R. Snow, M.L. Price, and J.P. Doty, DNA 5119F (June 1980).

10

A theoretical basis of CAT is given in Appendix A; as derived, the governing equation for deducing dust density is given below:

$$\rho_m = \frac{4}{3} \rho_g \beta \left[\frac{\int_{a\ min}^{a\ max} a^3 f(a)\ da}{\int_{a\ min}^{a\ max} Q(a)\ a^2\ f(a)\ da} \right] , \qquad (1\text{-}1)$$

where ρ_m is the dust mass concentration, ρ_g is the particle grain density, a is the radius of the dust particle, $f(a)$ is the particle size distribution function, and $Q(a)$ is the Mie parameter. The remaining symbol, β, denotes the attenuation coefficient due to atmospheric dust associated with the contrast between a target and its background; it derives from Koschmeider's Equation, viz.,

$$C = C_o \exp(-\beta R), \qquad (1\text{-}2)$$

where C, C_o are the apparent and inherent contrast, respectively, and R is the distance between the target and the observer. The MILL RACE CAT test consisted of six spaced photo targets at both the nominal 10 psi and 20 psi distance from GZ. In addition, there were three movie cameras at each location photographing the targets from just before detonation until several minutes after. By using Eqn. (1-2) for several different targets, we can derive the following basic equation:

$$\beta(t) = \frac{\ell n\ \dfrac{C_i(t)}{C_j(t)}}{R_j - R_i} , \qquad (1\text{-}3)$$

where i and j denote different targets and the range R_j is larger than R_i. The films of the six targets were analyzed by densitometry and the contrast for a given target at a particular time deduced by using the following equation:

$$C_i(t) = \frac{H_b - H_T}{H_b} , \qquad (1\text{-}4)$$

where H_b and H_T refer to the irradiance of the film due to the background and target, respectively, and are found from the measured density, D, of the developed film by use of the calibrated H & D curve associated with the particular film.

Once a temporal record has been found of at least two different photo targets, then Eqn. (1-3) can be used to obtain a temporal record of β. This was the fundamental objective of the CAT validation experiment.

11

Referring to Eqn. (1-1), the determination of absolute dust densities requires knowledge of the particle size distribtuion function as well as the Mie parameter. During the MILL RACE test, a separate experiment fielded by SAI (Reference 2) measured the particle size distribution vs time and the absolute dust mass concentration vs time at several locations directly in the line of sight between our cameras and photo targets. The particle size distribution function was supplied to us by SAI and we calculated the Mie parameter using a measured index of refraction value for the actual dust at the MILL RACE site. The grain density, ρ_g , was also measured for MILL RACE dust and along with our deduced value of β completes the terms on the right hand side of Eqn. (1-1); this immediately gives ρ_m (t). We can then compare the deduced value of ρ_m (t) found by the CAT with the measured value of ρ_m (t) found by SAI to determine the accuracy of the method.

Section 2 of this report describes the design of the experiment while Section 3 discusses the data obtained during the MILL RACE test. In Section 4, we compare the dust mass density deduced from the CAT with the measured data supplied by SAI. From this comparison we present the conclusions that we believe are warranted from the experiment. Several Appendices are attached showing the theoretical basis of the technique in more detail.

2. "Measurements of Dust Size Distribution and Dust Density at MILL RACE," J.E. Cockayne, SAI, (These Proceedings).

12

Table (2-1). Definition of parameters used in this Section.

PARAMETER	DEFINITION
T	Film running time
L	Film length
S	Camera speed
t	Exposure time
F	Frame rate
s	Sector
f	Focal length
γ	Slope of the emulsion characteristic curve
H	Film exposure
D	Film density
pps	Pulses per second

SECTION 2
EXPERIMENT DESIGN

2.1   OBJECTIVES

The Contrast Attenuation Technique validation experiment was planned to duplicate as closely as possible the test hardware used for many of the NTS atmospheric shots. Because the NTS atmospheric test series ended over 20 years ago, obviously it would be difficult to assemble the original personnel and equipment in the same configuration as used at that time. After some research and many helpful discussions with members of the Los Alamos EG & G office, we finally selected the company of HSS, Inc. in Bedford, Mass., to act as our sub-contractor in all of the experimental areas. This choice was based on HSS's intimate knowledge of NTS photographic data through actual experience. All of the key staff members at HSS who helped us in the MILL RACE experiment had been involved in on-site test participation at NTS in the photo-graphic experimental area. Not only did they have actual experience dating back to the atmospheric nuclear tests, but HSS also retained many of the same cameras that were used at those tests. In addition, HSS personnel have been activé in many other recent photographic tests involving H.E., rockets, satellites, etc., so their expertise continues into the present. Based on their performance at MILL RACE, we feel very fortunate in choosing HSS to assist us.

The experimental objectives of the MILL RACE validation test of the CAT were to obtain photographic data similar to NTS data showing the effects of shock-entrained dust obscuring known targets while at the same time an absolute measurement of the dust density was obtained. Then by comparing the dust densities deduced from the photographic data with the measured data, it would be possible to determine the accuracy of the CAT. Originally, TBE planned to conduct both the photographic and measurement tasks at MILL RACE. Because of several different reasons, the two tasks were split by DNA; SAI in McLean, VA. was contracted to perform the dust measurements while TBE conducted the photographic portion.

Data from previous high explosive tests, e.g., Dice Throw and Misers Bluff, were used to initially specify the test environment for MILL RACE.

15

Based on movies and data, we selected the locations for our two test stations at the nominal 10 and 20 psi distances from GZ. Originally, we were planning to use three test stations--one additional at 15 psi--but finally settled on two to minimize the number of dust measurement instruments which would be necessary. Since we planned to use six cameras for the three stations, we decided to continue with six even for two stations.

2.2   TEST SITE AND EXPERIMENT LOCATIONS

The MILL RACE shot was held on the White Sands Missile Range about twenty miles south of the Stallion Range Center which is at the northern boundary of the Base. Starting at ground zero, the terrain had a gentle slope rising towards the east. The Contrast Attenuation Technique Experiment was located in the northeast quadrant approximately between the 012° and 028° radial. Two different test stations were placed on the test bed--one at the $\sim$20 psi distance (228.6m) and the other at the $\sim$10 psi distance (298.7m).   Figure (2-1) shows a photo/layout of the 20 psi test station; the 10 psi station is shown in F ,ure (2-2). In both stations, the cameras were aimed towards the east

A test station consisted of two camera enclosures and six photo-targets. Since cameras have a straight line-of-sight. we obviously could not maintain exactly the same distance from GZ for all of the units. Therefore, we chose the camera enclosure containing the GSAP camera and the (1.83 x 1.83m) photo-target located 27.43m from the camera to be on the 20 psi or 10 psi distance. Using these reference points, the other five photo-targets were located as shown in Table (2-2).

The original design of the photo-targets and their locations was meant to provide a field-of-view to the GSAP cameras as shown in Figure (2-3). As shown, the horizontal spacing between targets was equal to the target's angular size while the vertical spacing was one-half the target's angular size. These dimensions were modified slightly because of the steel columns supporting the plywood sections. There was no impact of these columns on any data or analysis.

Height of the field-of-view was $\sim$1.52m above the ground. Since there was a slight upward slope to the ground as one moved from the cameras to the photo-targets, this meant a slight elevation to the field-of-view; the actual slope of the field-of-view was about two degrees for both stations. A final measurement was made of all of the relevant dimensions and these are shown in Table (2-3).

17

Fig.(2-1)   Photo showing layout of the 20 psi test station.

Fig.(2-2)   Photo showing layout of the 10 psi test station.

18

| Table (2-2) | | | Location of photo-targets on the MILL RACE test bed. Also shown are the differences in distance from GZ and the estimated difference in overpressure from the nominal 10 or 20 psi | |

Photo-Target	Distance from camera (m)	Size (m)	Nominal Range/ overpressure R/P (m/psi)	$\triangle R/\triangle P$ (m/psi)
1	3.05	.20 x .20	228.60/20	+ .57/- .15
2	5.18	.34 x .34	228.6/20	- .25/+.07
3	9.14	.61 x .61	228.6/20	- 1.58/+.41
4	15.24	1.00 x 1.00	228.6/20	+2.42/-.62
5	27.43	1.83 x 1.83	228.6/20	0/0
6	45.72	3.05 x 3.05	228.6/20	- 4.21/+1.07
7	3.05	.20 x .20	298.7/10	+1.53/-.05
8	5.18	.34 x .34	298.7/10	-0.19/+.02
9	9.14	.61 x .61	298.7/10	-1.50/+.15
10	15.24	1.00 x 1.00	298.7/10	+2.32/-.23
11	27.43	1.83 x 1.83	298.7/10	0/0
12	45.72	3.05 x 3.05	298.7/10	-4.66/+.45
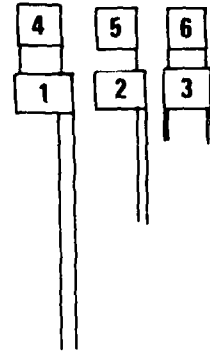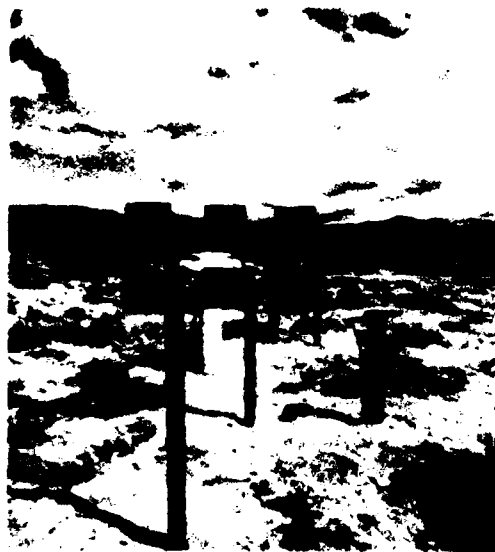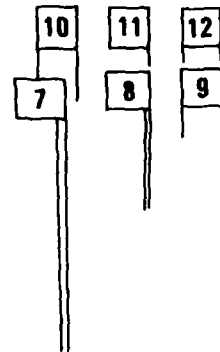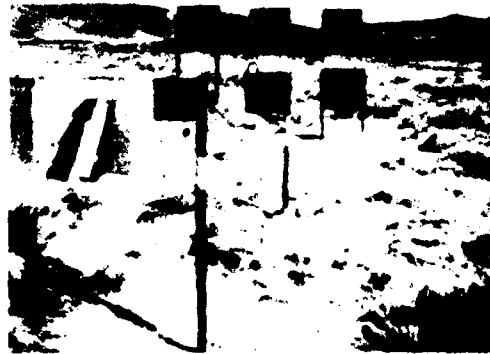
Figure (2-3)   Field-of-view of the GSAP cameras showing equal
angular dimensions of all photo-targets. The
top photo shows the 20 psi station while the
bottom photo shows the 10 psi station.

Table (2-3)   Measured distances to the photo-targets from the lens of the
              GSAP camera.

20 psi Station

Target	Distance from GSAP (m)	Height above ground (m)	
1	2.92	1.45	
2	5.05	1.39	Top of target
3	9.20	1.22	
4	15.16	1.58	
5	27.26	1.68	Bottom of target
6	45.74	1.65	

10 psi Station

7	2.90	1.44	
8	5.05	1.29	Top of target
9	9.14	1.20	
10	15.26	1.60	
11	27.00	1.58	Bottom of target
12	45.17	1.55	

By using the GSAP camera location as the reference point for locating the photo-targets, the field-of-view for the other two cameras at the same station will be skewed from that of the GSAP's. For the Flight Research camera, the distance between it and the GASP's was about twenty cm so that their fields-of-view were only slightly different. The Flight Research camera was able to see all of the photo-targets with sufficient spacing between them for contrast measurement.

However, the Mitchell camera's line-of-sight was displaced laterally almost 1.22 meters from the GSAP's. Due to this, the Mitchell's line-of-sight had almost total vignetting of the 2nd and 3rd targets by the 1st target; the farthest three targets were not affected to any appreciable degree.

2.3   PHOTO-TARGETS

The photo-targets consisted of twelve plywood squares (six each at the 20 psi and the 10 psi stations) and of dimensions and distance from the cameras as shown in Table (2-2). Although both stations used identically sized wooden squares for photo-targets, the frames and supporting columns were constructed from different size material depending upon whether the target was placed at the 20 psi or the 10 psi distance. Because damage occurred to the largest target (3.05m x 3.05m) at the 20 psi station, a description of that particular unit will be given below.

The frame for the large plywood section was made from 12.7cm (5") nominal ID standard weight steel pipe with 5.08 x 5.08cm (2"x 2") x .48cm (3/16") angle legs welded to the pipe in sections of from 30cm to 68cm in length. Prior to the detonation, an examination of this photo-target (as well as the others) indicated very close alignment of the radial emanating from ground zero with the plane of the plywood target. If a perfectly normal shock wave had arrived at this target, the only cross-section to intercept the pressure wave consisted of the 5" ID pipe on the windward column; therefore, one would expect any damage to be in a radial direction away from GZ.

All of the photo-targets and supporting members were painted prior to the explosion with a high-quality flat black paint. The intent was to make the targets appear to be ideal black bodies throughout the spectral range of the film. Figure (2-3) shows the photo-targets in the field-of-view of the GSAP cameras prior to the test. Unfortunately, events occurring during the actual HE test severely modified our carefully prepared surface and eliminated the black body hypothesis.

23

2.4   CAMERAS

Three different camera types were used at both the 20 psi and the 10 psi station. A Mitchell HS-100 high-speed 35mm camera and a Kodak GSAP (Gun Sight Aiming Point) 16mm camera were chosen as identical to cameras used during NTS shots. In addition, a Flight Research IV C 35mm camera was also used for several reasons:

1. To provide redundancy for the Mitchell camera.
2. To obtain data on a more recent vintage camera.
3. To obtain 35mm data at approximately the same location as the 16mm GSAP in order to compare film characteristics.

All cameras were set with a lens focus at infinity for all runs.

2.4.1   Mitchell 35mm Camera

The Mitchell cameras, made twenty-five or thirty years ago, are large, high quality, professional movie cameras that have complex mechanisms and are powered by 110V A.C. electric motors. Film magazines for this camera handle up to 152m. film lengths which was longer than the other two camera's maximum film length. Film running time, T, can be calculated as follows:

$$T = \frac{L\ F}{S} \tag{2-1}$$

where L is the film length in meters, S is the camera speed in frames/sec, and F is the number of frames per meter. For 35mm film F = 52.5. Thus for the Mitchell cameras,

$$T = \frac{8 \times 10^3}{S} \text{ seconds,}$$

or

$$T = 333 \text{ seconds at } S = 24\,\frac{\text{frames}}{\text{sec}} ,$$

the speed used during the MILL RACE tests. Assuming a nominal value of 10 seconds to obtain the 24 frames/sec speed after turning the Mitchell's motor on, we find

$$T = 323 \text{ seconds} = 5 \text{ min } 23 \text{ sec}$$

as the total film time available for data gathering. (Actually the test time was slightly greater than this because the camera was operating at less than 24 frames/sec during the initial 10 seconds i.e., accelerating

from zero to the final speed. Therefore the amount of film exposed during this 10 seconds was less than the 5 meters calculated using a constant speed of 24 frames/sec and thus there was more film available during the data gathering time).

An important feature on the Mitchell cameras not included on either the Flight Research or the GSAP cameras were timing marks placed on the film at a 50pps rate. A TD-60 Timing Mark Generator was used to provide accurate timing signals which were then used to fire spark markers. The timing mark was located on the outer edge of the Mitchel film and after processing provided a means for determining the time at which an event occurred on the film. The use of spark markers instead of neon bulbs was mandated by the low ASA number of the 3414 film. During pre-liminary tests at HSS, Inc., the neon markers normally used on the Mitchell cameras, were not able to expose the film sufficiently and thus were not visible after processing. Not coincidentally , during the atmospheric nuclear testing, all of the Mitchell cameras were adapted to spark marker systems in order to expose the MF film used for most of the shots because it also had a very low ASA number.

Exposure of film inside a Mitchell camera can be controlled using several independent settings. The frame rate, F, shutter opening (f/stop), and sector, s, all determine the exposure. The exposure time, t, is given by

$$t = \frac{1}{F}\left(\frac{s}{360}\right).$$

(2-2)

For the MILL RACE shot, the frame rate was 24 $\frac{\text{frames}}{\text{sec}}$ and the sector was 170°. Therefore

$$t \sim .02 \text{ sec} = \frac{1}{50} \text{ sec.}$$

Both Mitchell cameras used a 35mm Baltar lens.

The f/stop determined by pre-shot testing was f/3.5 for the 10 psi Mitchell and f/2.8 for the 20 psi Mitchell.

2.4.2. Kodak GSAP 16mm Cameras

The Gun Sight Aiming Point cameras, manufactured by Kodak, were of WWII vintage. Due to their small size, ruggedness, low-cost, and simplicity, a large number were used during the atmospheric nuclear test-ing program. Most of the NTS film library consists of 16mm records taken with GSAP cameras. Therefore, we placed great emphasis on obtaining data

using GSAP cameras at MILL RACE. The cameras themselves were veterans of several NTS shots. As expected, these cameras were trouble-free and produced relatively high quality data in spite of their age. Because we were unable to procure the Type 3414 Film in 16mm size, we used Kodak Type 2476 film in 15.2m rolls which had the same spectral response but a much higher ASA number. Both of the GSAP cameras were run at 16 frames/sec with a sector of 130°. The corresponding exposure time, t, is given by

$$t = \frac{1}{F}(\frac{s}{360}) = \frac{1}{16}(\frac{130}{360}) \simeq .02 \text{ sec,}$$

or

$$t = \frac{1}{50} \text{ sec; the same as the Mitchells'.}$$

Since 16mm film has 131.2 frames/m, the total running time for the GSAP cameras was

$$T = \frac{LF}{S} = \frac{(15.2)(131.2)}{16} = 125 \text{ seconds.}$$

Unlike the Mitchell cameras, the GSAP required a very short acceleration time so that the available data gathering time was practically identical to T. There were no timing marks placed on the GSAP's film during the run but speed tests conducted prior to MILL RACE determined the fixed framing rate for both cameras. Therefore, it was simply a matter of measuring the distance along the film to determine the exposure time of any particular event. The lens used in the GSAP cameras were Bell and Howell Super Comet with a focal length of 17.8mm. During MILL RACE the GSAP's were run using f/stops of f/19 and f/16 for the 10 psi and 20 psi cameras, respectively.

2.4.3. Flight Research Cameras

The Flight Research 35mm cameras are of fairly recent design, and classify as relatively simple units about one-third the size of the Mitchell camera. Because of their compact size, it was possible to place the Flight Research cameras in the same enclosure as the GSAP cameras so that their fields-of-view were essentially identical. This allowed for a direct comparison during film analysis of the Type 3414 and 2476 Kodak films.

Framing of the camera was controlled by a fixed speed motor and gear selection for speed control. During the MILL RACE tests, they were run at 10 frames/sec and set for a sector of 72°. Thus the exposure time,

26

t, is given by

$$t = \frac{1}{F} \left(\frac{s}{360}\right) = \frac{1}{10} \left(\frac{72}{360}\right) = .02 \text{ sec}$$

or
$$t = \frac{1}{50} \text{ sec.}$$

The data gathering time, T, is found from

$$T = \frac{LF}{S} \quad ;$$

shot runs at MILL RACE used 21.3m rolls of 3414 film so

$$T = \frac{(21.3) \ (52.5)}{10} = 112 \text{ sec.}$$

The Flight Research cameras used 35mm Camera Equipment Corp. lens with an f/stop of f/3.5 for both the 10 psi and 20 psi station.

2.5   FILM

The film used during the NTS nuclear testing was Kodak Type Micro-file for most of the shots. This film was especially specified for use in a nuclear environment because of its low sensitivity to gamma radiation. One side effect of such a specification was a very low ASA rating for this film (ASA 1-3). Kodak no longer manufacturers this particular emulsion so an extensive investigation was made of the available films to find the best substitution. Aiding in this search was Mr. Charles Wyckoff who was a major contributor to the initial specification of the MF film. He recommended Kodak Type 3414 film as the best substitute for the MF film based on very similar, if not identical, spectral response functions. The major differences between the two films was apparent in the curves showing film density vs exposure for various choices of γ (the slope of the emulsion char-acteristic H&D curve); the MF film had a much larger latitude. Mr. Wyckoff believed that this difference would be minimized by using suitable processing techniques and would not pose any problem in analyzing the film data for our tests.

Data for type 3414 film is shown on the accompanying data sheets supplied by Kodak (see Appendix C). Upon selection of this film, we con-tacted Kodak for price and delivery information. The result of our inquiry was an order for sixteen rolls of 35mm film in 152.4m lengths. It was not feasible to purchase any 16mm film with 3414 emulsion and for a while we were even apprehensive about obtaining the 35mm film in time for MILL RACE. This last fear proved negative and we received the ordered film a month prior to the MILL RACE fielding.

However, we still had to choose the 16mm film for use in the GSAP cameras. Again Mr. Wyckoff assisted in the selection and recommended use of Kodak Shellburst Film #2476. As evidenced on the accompanying data sheets, the main difference between 3414 and 2476 lies in the exposure index with values of 2.5 and 250, respectively. Their spectral response functions although not identical, are very similar.

After deciding upon 2476 film for our use, we contacted Kodak only to learn that they were completely out-of-stock for this film and were not planning to manufacture additional units for six months. With the assis-tance of the MILL RACE Test Staff, we finally located and procured sufficient quantities of 16mm 2476 film through the WSMR photographic department.

2.6   POWER AND CONTROL

The power and control system used for the CAT validation experiment is shown in Fig. (2-4). Except for the two camera enclosures, the remaining units were placed inside an excavated pit next to the enclosures and covered with sandbags prior to detonation. A number of foam sheets were placed under and around the units to provide some shock protection.

Power to the cameras was provided by commercial-type automobile batteries newly procured for the test. Battery charging was performed as necessary and was accomplished by having two sets of batteries, one being charged while the other was used.

The cameras were turned on by a relay closure circuit provided by Field Command. This signal was used to activate our control unit which had a latching relay to keep power applied to the cameras even after the relay closure provided by Field Command was disabled. Thus we planned to activate our cameras beginning at 10 seconds prior to detonation and keep them on until we arrived at the test stations and manually disabled them.

The Mitchell cameras had a built in timing mark generator to provide a known reference. This unit was controlled by a TD-60A film marker set to operate at 50 pps.
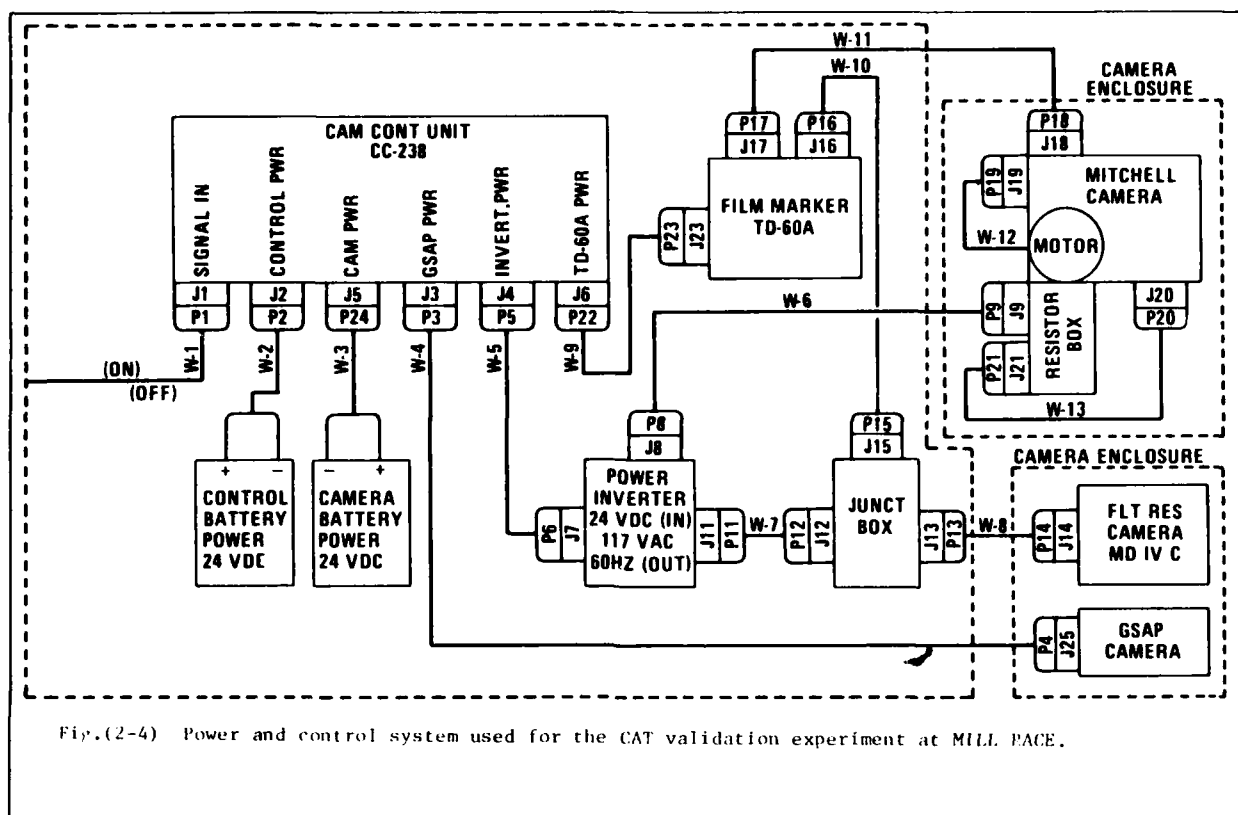
Fig.(2-4) Power and control system used for the CAT validation experiment at MILL RACE.

SECTION 3

DISCUSSION

3.1   TEST RESULTS

The MILL RACE explosion occurred at about 1235 on Sept. 16, 1981.
All of our cameras operated as planned except for the Mitchell at 10 psi
which jammed after about one half of the film was exposed. Damage occurred
to the largest photo-target at the 20 psi station; also, the Mitchell cam-
era enclosure at 20 psi was slightly tilted due to the force of the shock
wave, but a boresight check of the camera indicated that all of the photo-
targets were still within its field-of-view. Post-test examination revealed
that all the photo-targets at the 20 psi station and the three smallest at
the 10 psi station were coated with a thin layer of dust which was embedded
on the painted surface. It was obvious that these targets no longer approx-
imated an ideal black surface. By using two calibrated reflection cards,
we estimated the surfaces to have a reflection of between (0.2-0.3).
Fig. (3-1) and (3-2) show post-test photos of the photo-targets at the two
test stations.

During removal of the equipment after the experiment was completed,
we discovered the TD-60A units at the 20 psi station had received a sizable
shock which resulted in the disconnection of several circuit boards. Most
likely, the ground shock from the detonation caused this and ended the
timing mark generation at about shock arrival time.

The data film were carefully removed and packed for shipment to
the processing laboratory. Under the supervision of Mr. Charles Wyckoff,
a step wedge filter was used to expose identical film and along with the
data film, processed according to the technique indicated below.

Fig.(3-1) Post-test photo-targets at 20 psi.
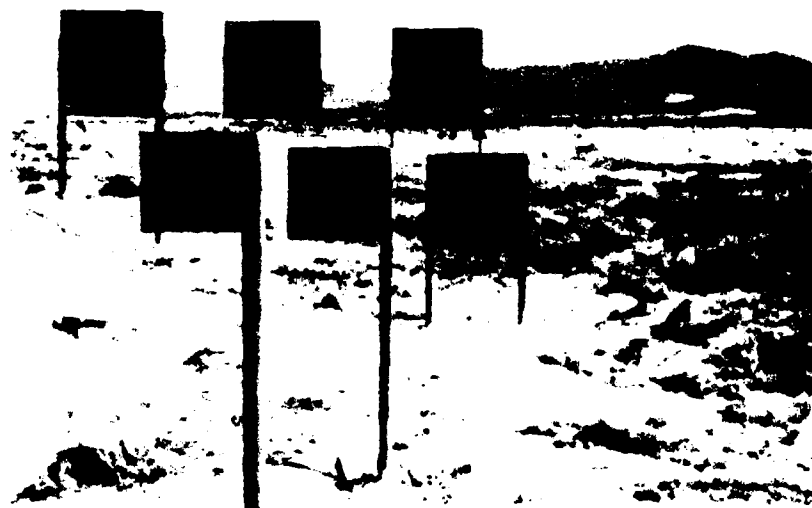
Fig.(3-2) Post-test photo-targets at 10 psi.

3.2   FILM PROCESSING

3.2.1   Sensitometry and Film Development

3.2.1.1 Processing (General)

Eight shot films of two different black & white film stocks were processed by Film Facts Engineering (FFE) Inc. in a Kodak Versamat 11C-M. All films were proceeded by and accompanied by sensitometric step control scales using identical emulsion stock. An EG&G Xenon Flash Sensitometer was used to expose the control and check scales.

The Kodak Versamat 11C-M is a continuous processing eleven inch wide film machine with a large variety of processing controls such as temperature, speed drive variation, continuous heating and cooling developer temperature, balancing of the developer with constant filtering, operator's option of replenishing the developer and fixer solutions with fresh solutions before, during or after processing in accordance with the amount of film processed.

3.2.1.2. Sensitometry

FFE, Inc. used an EG&G Xenon Flash Sensitometer Mark VII to expose a calibrated step scale on to fresh film stock of the same emulsion batch used for the record film. A test scale was processed before any record film was run or processed in the machine. The test scale was read on a Macbeth Quantalog Densitometer. Measurements were plotted to determine if the processing machine controls, i.e., speed, temperature, drying, fixation and washing were all satisfactory for processing the film. When the record film was to be processed, a scale was placed at the head and at the tail of the film. It was rarely possible to place the control scale directly on a shot film. An alternative was generally taken; control scales were made and run at the head and tail of the record film. Two records were kept of the machine processing conditions; one in a processing log in the machine room and the other on the plot of the control scale (density vs log-exposure). The results of measurements taken for the two Flight Research and one GSAP cameras are shown in Figs. (3-3), (3-4) and (3-5). (Note that the units shown along the abscissa are not absolute exposure units but merely abitrary units that were useful for film calibration.)
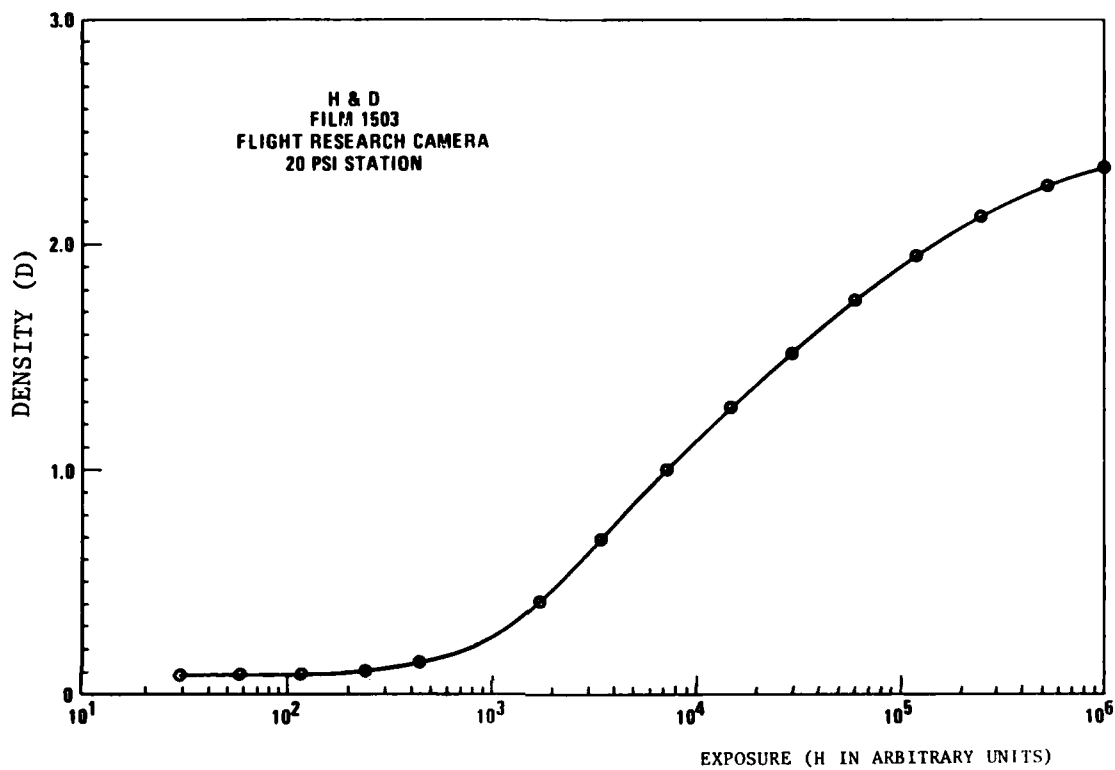
FIG. (3-3) Calibration Curve for the Flight Research Data Film at 20 psi
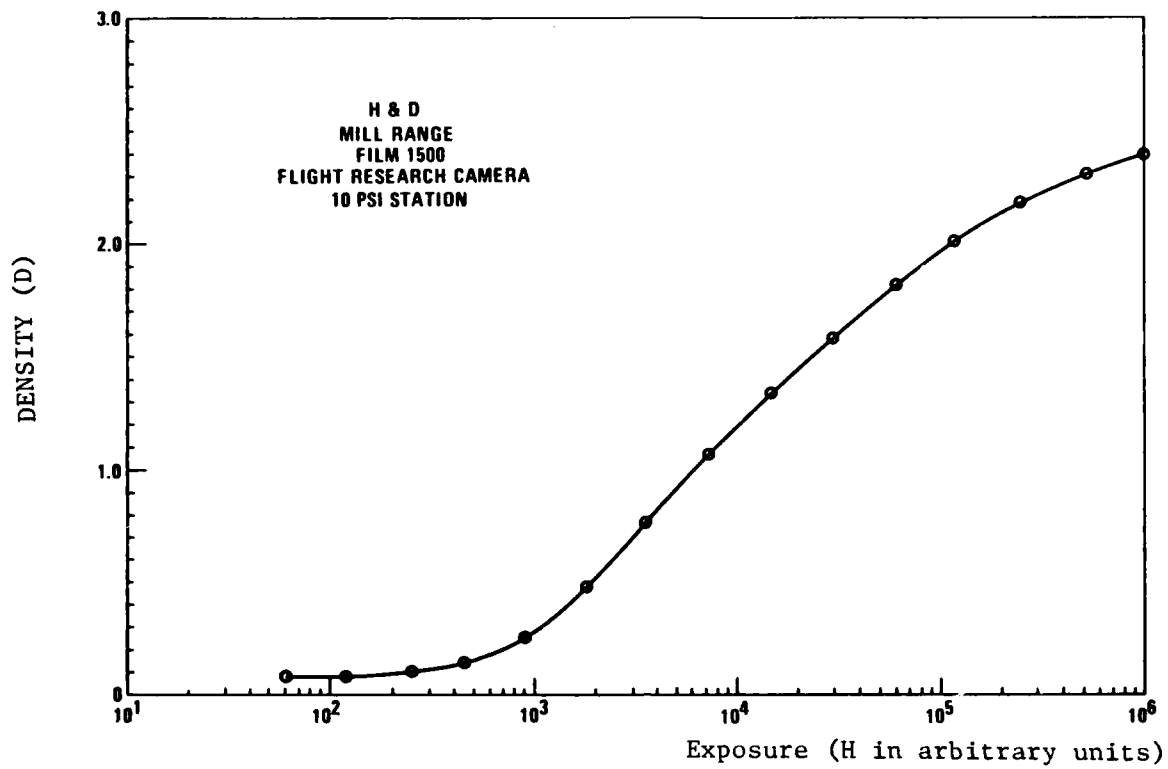
FIG. (3-4) Calibration Curve for the Flight Research Film at 10 psi

36
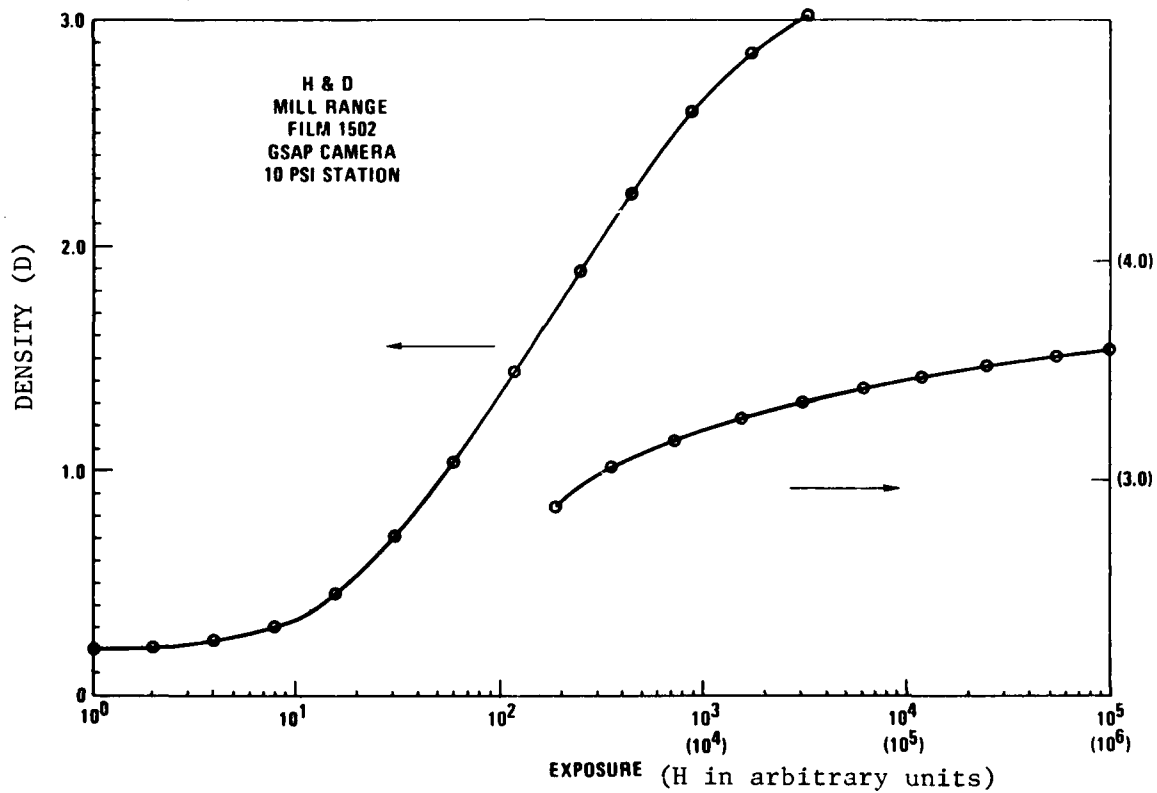
FIG. (3-5) Calibration Curve for the GSAP Camera Data Film at 10 psi

3.2.1.3 Film Development

There were two types of shot films used: Kodak High Definition Aerial Film (3414-1751021 35mm), Estar base; and Kodak Linagraph Shellburst Film (2476-49335 E 16mm) Estar base. Kodak's published data for processing of these films in a Versamat processor was limited to very specific processing conditions. For example: the 3414 emulsion characteristic curves were specific to Versamat 885 chemicals, one developer rack and speeds of 10 ft/min and 15 ft/min; no emulsion characteristic curves were given for the type 2476 using Versamat processing; however, the gamma of the curves was given for three Versamat chemistries Type A, Type 885 and Type 641. The information supplied by Kodak was of little value because their processing specifications led in every case to high contrasts and short exposure latitudes for both films. As a result, it was necessary, under the guidance of Mr. Charles W. Wyckoff--a recognized expert in film processing--to experiment with various processing chemistries and processing conditions.

The processing machine options available required both close monitoring and regular sensitometric checks. Many different developers and processing conditions were tested to achieve optimum performance for a given application with a unique combination of developer, time and temperature. Variance from these conditions will yield less than optimum results due to: alteration of base fog level, loss of film sensitivity, increase in grain size, incomplete development, chemical residue left in the film, or improper drying.

The optimum chemistry to achieve the desired MILL RACE Film characteristics was found to be Kodak Type-B Chemistry with a slightly modified pH value. Two developer racks were required. Optimum developing temperature was $87^{o}F$. Optimum film speeds differed for the two emulsions. Exact processing conditions for each of the eight films are given in Table (3-1).

Adjacency and Bromide Drag effects are problems that constantly trouble photometric photography. The adjacency effect is a problem associated with two or more images which lie close together. Prolonged or irregular development can cause loss in density of one or both images or a buildup of density between the two images. This effect was minimized or eliminated in the Versamat 11C-M by proper maintenance of the machine and development of the film in the mid-ranges of the drive speed which goes from 0 to 25

Table (3-1). Processing Conditions for the MILL RACE Films.

Machine: <u>Versamat 11C-M</u>   Developer: <u>Modified Type B</u>

Date	Film Perforation Number	Emulsion Type	Film Size (mm)	Developer Temperature (°F)	Machine Speed (ft/min)
28 Sep 81	1500	3414	35	87	6
29 Sep 81	1501	3414	35	86	6
	1506	3414	35	87	6.5
	1503	3414	35	87	6.5
	1504	3414	35	87	6.5
6 Oct 81	1502	2476	16	87.5	8
	1505	2476	16	88	8
	1507	2476	70	88	8

feet per minute. In addition, the machine had certain of the rollers slightly overdriven to eliminate film slack due to normal film stretching. Bromide buildup in the developer is caused by an imbalance of excessive amounts of image processing in relation to amount of replenisher being fed to the developing tank. Bromide drag problems were eliminated in this machine through proper replenishment techniques, recirculation of the developer, filtering of the developer, and sensitometric checks on development.

Agitation of the Versamat 11C-M was derived from the movement of the film itself through the developer tank, assisted by chain-driven rollers which in turn drove or propelled it and/or churned the adjacent developer to drive fresh developer on to the surface and at the same time drive the used developer away from the film emulsion surface. The only other motions in the developer tank were the recycling of the developer exiting to the cooling and heating chambers to maintain constant temperature of the eight gallons in the machine processing tank, and a trickle input of fresh replenisher developer stock. The machine operator had mechanical controls of this vital process for heating and cooling of the developer and to control the drive speed of the machine for the time of film development. These controls yielded the total development gamma resultant on the film.

3.2.2   Film Densitometry

After all of the films were processed, we spent considerable time
examining each film using a Moviola film display unit. All three cameras
at each station had good data showing the effects of dust on the contrast
of the photo-targets. Because the Mitchell camera's field-of-view did not
clearly delineate the three closest targets and their backgrounds, and due
to the loss of timing marks at shock arrival time, we decided to use the
Flight Research 35mm films as our prime source of data for densitometry
measurements. The GSAP cameras would be used at selected points to obtain
data on the 16mm 2476 film for correlation with the 35mm 3414 film.

Once the decision to use the 35mm Flight Research film for densito-
metry was made, we chose two different densitometers to use for the analysis.
The amount of data available was considerable; one Flight Research camera
alone had over 1000 frames of exposed film. Clearly, we needed a fairly
quick method for measuring the density of the film for each target and its
associated background. However, there was interest in more detailed study
of selected frames on the uniformity of the dust and/or to measure the dust
gradient across an individual target. To accomplish both the quick analyses
as well as the detailed dust profile studies, we selected two different den-
sitometers: the Macbeth Quantalog Densitometer provided a diffuse density
measurement in that an average film density over $\simeq 1mm^2$ was measured using
a manually controlled scanning system for both the target and its background;
the Photometric Data Systems Model - 1000 provided a microdensitometer scan
using a beam with an area of $\simeq 4 \times 10^{-3}$ mm^2 and a digitally controlled scan-
ning motor. More information is provided below on each of these instruments.

3.2.2.1 Diffuse Density Measurements of MILL RACE FILMS

        Diffuse density measurements of the targets and backgrounds on the
MILL RACE photographic films were made with a Model TD-102 Macbeth
Quantalog Densitometer.

        All diffuse density measurements using the TD-102 were made with
a circular aperture 0.046 inch (1.17mm) in diameter. This aperture was
the smallest aperture which could be employed with the TD-102 while main-
taining a valid calibration of the instrument. Target images on the Flight
Research IV C and Mitchell HS-100 Camera 35mm records were approximately 2 mm x
2 mm in size; the measuring aperture of the TD-102 could comfortably fit
within these target images. On the other hand, target images on the GSAP
Camera records were about 1 mm x 1 mm in size. Because the GSAP images
were smaller than the densitometer aperture it was not possible to make
diffuse density measurements on the GSAP films with the TD-102. (Note:
the primary reason for using the TD-102 rather than the micro-densitometer
for the contrast measurements was that the TD-102 permitted large quantities
of data to be processed in a reasonable amount of time.)

        Figure (3-6) illustrates the locations on the Flight Research Cam-
era records where diffuse density measurements were made. Background
measurements made at positions B1, B2 and B3 were intended for use with
targets T1, T2 and T3, respectively. They could also be used for deter-
mining target contrasts with targets T4, T5 and T6 if the situation permitted.
At late times, if the optical thickness of the atmospheric dust along
lines-of-sight B1, B2 and B3 was not infinite (i.e. desert terrain was
showing at these locations) then the background measurements at positions
B4, B5 and B6 could be substituted for use with targets T4, T5 and T6
respectively.

        Apparent target contrasts, C, were determined in the manner outlined
in Figure (3-7). An emulsion characteristic curve (H&D) generated from a
sensitometric step wedge using the TD-102 densitometer was used to convert
the target and background film densities to relative brightness values.
(The sensitometric step wedge was processed under carefully controlled
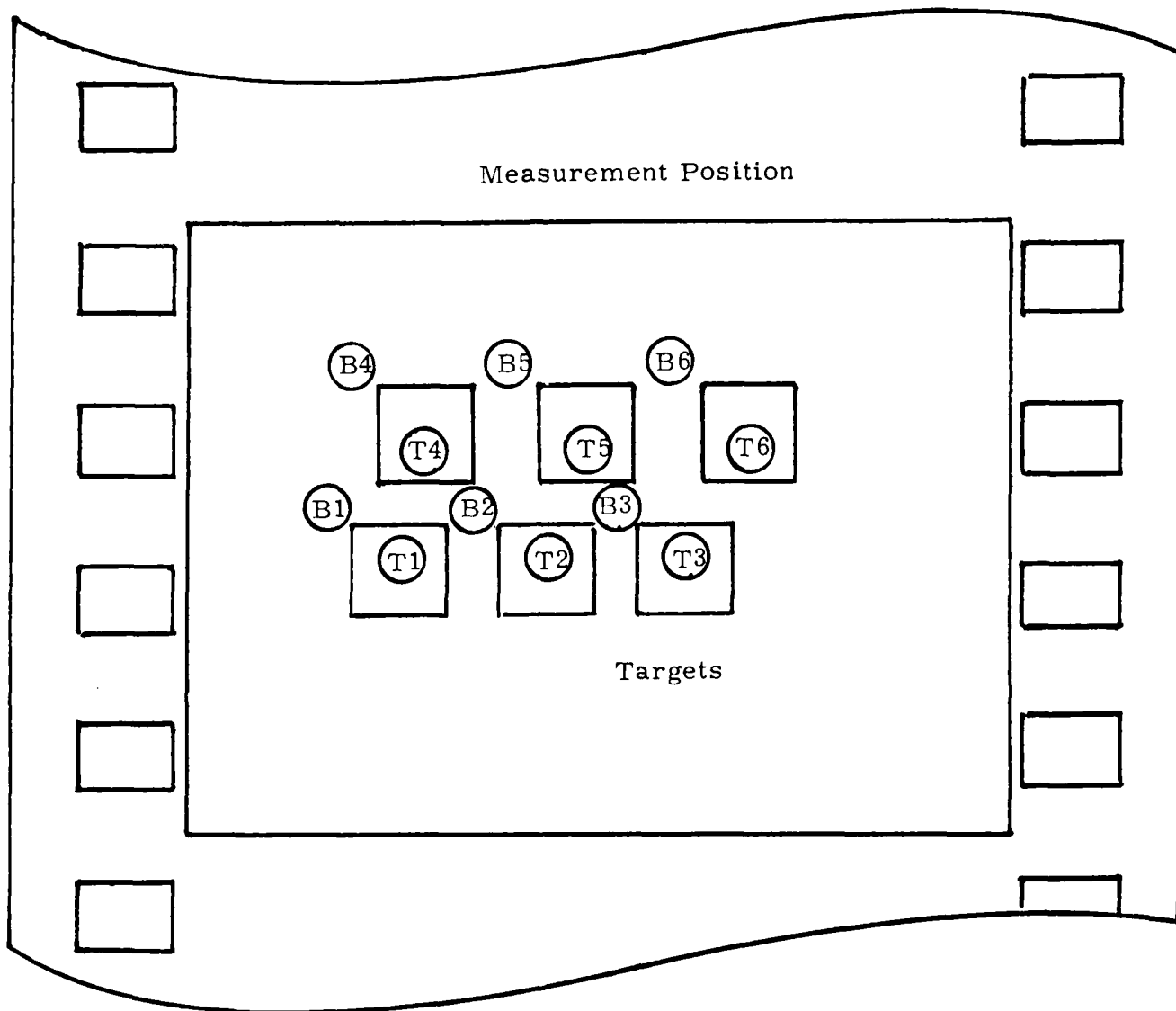
Figure (3-6). Location of density measurements on Flight Research camera records.

DATA FILM		SENSITOMETRIC STEP-WEDGE

DIFFUSE DENSITY MEASUREMENTS

Mac Beth Quantalog Densitometer Model TD-102

FILM DENSITIES TARGETS AND BACKGROUND	EMULSION CHARACTERISTIC CURVE

RELATIVE BRIGHTNESS OF TARGETS AND DUST BACKGROUNDS	TARGET (B_t) BACKGROUND (B_b)

APPARENT CONTRAST BETWEEN TARGET AND DUST BACKGROUND	$C = \dfrac{B_b - B_t}{B_b}$

EXTINCTION COEFFICIENT OF DUST BETWEEN TARGETS $(i = 1 \rightarrow 5)$	$\beta = \dfrac{1}{(R_{i+1} - R_i)} \ln \left(\dfrac{C_i}{C_{i+1}} \right)$

Figure (3-7). Outline of procedure for obtaining optical extinction coefficients of atmospheric dust from MILL RACE films.

conditions along with the data film, using development and agitation techniques designed to overcome all edge-effects and bromide-drag effects).

The relative brightness values were then used to determine the apparent contrast of any given target using as the defining relation for apparent contrast

$$C = \frac{B_b - B_t}{B_b}$$

where B_t is the relative brightness of the target and B_b is the relative brightness of the adjacent dust background.

The optical extinction coefficient β of the atmospheric dust between any part of targets was determined from the relation

$$\beta = \left(\frac{1}{R_j - R_i}\right) \ln \left(\frac{C_i}{C_j}\right) \qquad j > i \qquad (1-3)$$

where i designates any target 1 through 5, and j designates any target 2 through 6.

3.2.2.2 Microdensitometer Scanning of MILL RACE Films

To supplement the diffuse density measurements made on the MILL RACE films with the Macbeth Densitometer and to examine spatial variations in the target scenes, scans of selected frames were made on a recording microdensitometer. This type of densitometer measures specular density rather than diffuse density and a separately determined H&D curve measured by the instrument itself must be obtained. While the corresponding density measurements between the two methods cannot be compared, the relative exposure values obtained using the respective H&D curves can be directly compared.

The microdensitometer used for these scans was Photometric Data Systems Model-1000 (PDS-1000). In this instrument the film was mounted between clear glass plates which sit on a platen driven in an x-y rectangular coordinate system by two digital step motors. The minimum step in either direction was 2 microns. The motors could be driven continuously or with single steps. They could be manually operated from front panel switches or automatically programmed by an auxiliary control system.

A variety of scanning apertures was available on a rotating wheel A 71 micron diameter circular aperture was used in all of the scanning done on these films. The optical system was in the form of a single beam transmissometer whose output voltage was converted to density by an electronic logarithmic amplifier. The resulting analog voltage output could be recorded on a chart recorder or converted to digital output and recorded on a magnetic tape.

For these scans, the analog density output was recorded on a Brush Recorder Mark 250 which gave an ink record on a 11.43cm (4½") wide paper chart with an imprinted precision rectilinear grid graduated in 50 divisions for the 4½" width.

The experimental procedure started by mounting the film on the platen between clear glass plates and aligning the film with the x-y scanning coordinate system. The optical system was focused and the transmission output was set to read unity on a front panel digital voltmeter when the light beam was passing through clear glass. The output was then

switched to read density and the density scale was set using calibrated v... Density filters mounted on an internal rotating filter wheel which intercepts the optical beams. Next, the recorder scale was adjusred to read density as displayed on the front panel digital meter. All of the electronic settings were reset before each scan. The platen scanning speed and the chart speed were chosen to give a suitable record length The recorder amplifier was set to give near full scale density readings for each scan. When the density varied widely during a scan, the measure ment was repeated using a different recorder setting in order to on... good readings at all points.

3.3 CONTRAST MEASUREMENTS

The measured film density found using the densitometer converts to an exposure value by using the H and D calibration curve. For a given film frame, each target that was visible had a pair of exposure values assigned to it--one for the target and one for the background. These exposures related directly to the apparent brightness of the target and its background. Thus, we define the contrast of a target, T, at distance R by the following expression:

$$C(R) = \frac{B_b - B_T}{B_b}, \tag{3-1}$$

where B_b and B_T refer to the brightness of the background and the brightness of the target, respectively. Since the brightness and the exposure were linear in this application, we substituted one for the other in determining the contrast, i.e.,

$$C(R) = \frac{H_b - H_T}{H_b} . \tag{3-2}$$

The contrast for a given target at a given time was found by using the measured exposure value for the target and its background along with Eqn.(3-2). Both of the Flight Research films were analyzed out to 60 seconds after shock arrival. An analysis shown in the next section derives a few simple selection rules used for deciding which targets would produce the best data when multiple targets were visible.

The background exposure on the film was determined by many factors. All sources of light such as direct sunlight, scattered light, reflected light, and emitted light from any object contributed to the background brightness. An equation for the background brightness, B_b, is given in Eqn.(3-3).

$$B_b = \int_0^\infty H\phi\sigma\exp\left[-(\beta_{ext}r)\right] dr, \tag{3-3}$$

where H is the total airlight at a distance r, (see Fig. (A-1), σ i. the total scattering coefficient, ϕ is the angular dependence function of σ. and β_{ext} is the extinction coefficient. When H, ϕ and β_{ext} are uniform between the camera and r, we can integrate Eqn. (3-3) and obtain the fo lowing term:

$$B_b = \frac{H}{\beta} \frac{\phi \sigma}{\beta_{ext}} \cdot$$

(3-4)

Eqn. (3-4) applies for optically dense media, such as heavy dust concentrations, when $(\beta_{ext} r) >> 1$. Even when Eqn. (3-4) can be used, however, the background radiance in general will be changing with time as H, ϕ and β change.

Contrast was defined by Eqn. (3-1). If the target radiance was zero, which would occur for an ideal black target, then the inherent contrast would equal:

$$C_o = \frac{B_b - 0}{B_b} = 1*$$

(3-5)

for all values of B_b. This was the initial objective of our MILL RACE experiment design; we carefully painted all of our targets with a high quality, flat black paint in order to satisfy Eqn. (3-5). Unfortunately, the surfaces of the targets were significantly modified by a layer of dust embedded into the paint sometime during the passage of the dust cloud. The resulting surface no longer approximated an ideal black surface but probably had an refectivity of between (20-30)% based on post-test measurements. Therefore we could not use the simple term for C_o given by Eqn.(3-5) but must return to Eqn.(3-1) for our analysis.

*The convention of C_o = +1 for a black object is widely although not universally used; some use C_o = -1.

Selection Rules

The Contrast Attenuation Technique for determining dust density is
d on Koschmeider's Equation, viz.,

$$C = C_o \exp(-\beta R). \qquad (3\text{-}6)$$

In the MILL RACE experiment, it was previously shown that for multiple
targets, a modified form of Eqn. (3-6) produced better results, e.g.,

$$\frac{C_i}{C_j} = \exp\left[\beta(R_j - R_i)\right], \quad i<j. \qquad (3\text{-}7)$$

We will examine the use of Eqn. (3-7) for analyzing the MILL RACE
films and derive a few simple "Selection Rules" to use with the data to
minimize processing errors.

Let us redefine Eqn. (3-7) with the following independent variables:

$$\frac{x}{y} = \exp\left[\beta(R_y - R_x)\right] \qquad (3\text{-}8)$$

where x and y are two contrasts for different targets on the same frame as
measured from any of the MILL RACE film.

Solving for β, we find

$$\beta = \frac{1}{R_y - R_x}\left[\ell n\ x - \ell n\ y\right]. \qquad (3\text{-}9)$$

Consider a small incremental change in β and its relation to both x and y,
i.e.,

$$\Delta\beta = \frac{1}{R_y - R_x}\left[\frac{\Delta x}{x} - \frac{\Delta y}{y}\right]. \qquad (3\text{-}10)$$

Divide both sides by Eqn. (3-9) to obtain,

$$\frac{\Delta\beta}{\beta} = \frac{\left[\dfrac{\Delta x}{x} - \dfrac{\Delta y}{y}\right]}{\ell n\ x - \ell n\ y}. \qquad (3\text{-}11)$$

The error in Δx and Δy (ΔC_i and ΔC_j) were determined by the film processing
and the resolution of the densitometer used in measuring the contrasts.
Both of these factors remain constant for a given film and a densitometry
measurement of the same film frame. Therefore we can equate Δx and Δy; thus,

$$\left(\frac{\Delta\beta}{\beta}\right) = \left(\frac{y - x}{xy}\right)\left(\frac{1}{\ell n\ \dfrac{x}{y}}\right)\Delta C, \qquad (3\text{-}12)$$

where we define $\Delta C = \Delta x = \Delta y = $ Constant.

The term on the left of Eqn. (3-12) is the incremental error in the deduced extinction coefficient due to the measured target contrasts for two targets x and y. The minimum error occurs when

$$\frac{\partial}{\partial C} \left(\frac{\Delta \beta}{\beta} \right) = 0. \qquad (3-13)$$

After differentiating the right hand side of Eqn.(3-12) (and some messy algebra) we find the following expression:

$$\frac{\frac{x^2}{y^2} + 1}{\frac{x^2}{y^2} - 1} = \ell n \left(\frac{x}{y} \right). \qquad (3-14)$$

Solving Eqn. (3-14), we find that

$$\frac{x}{y} \simeq 3.01, \qquad (3-15)$$

will minimize the error in $\frac{\Delta \beta}{\beta}$.

Or

$$\frac{C_i}{C_j} \simeq 3.01 \quad ,$$

$$C_i = (3.01) C_j \quad , \qquad (3-16)$$

$$\ell n \, C_i = \ell n \, C_j + 1.10 \quad .$$

From Eqn.(3-9), we have for minimum error,

$$\beta = \frac{(1.10)}{R_j - R_i} . \qquad (3-17)$$

Although Eqn. (3-17) gives the best ratio of C_1 and C_j, it does not give any guidance in selecting the best values for both C_i and C_j. We can derive this by looking at Eqn.(3-6) ,

$$C = C_o \exp(-\beta R).$$

or

$$\beta = \frac{1}{R} \, \ell n \left(\frac{C_o}{C} \right) \quad . \qquad (3-18)$$

51

By following a similar argument as used to derive Eqns. (3-11) to (3-16), we can derive the following equations:

$$\frac{\Delta\beta}{\beta} = \left(-\frac{1}{(\ln C - \ln C_o)}\right)\left(-\frac{\Delta C}{C}\right) \tag{3-19}$$

$$\ln\left(\frac{C_o}{C}\right) = 1, \tag{3-20}$$

$$C = C_o e^{-1},$$

or

$$C = (.368)C_o. \tag{3-21}$$

Returning to Eqn. (3-12) and using the results given in Eqn. (3-15), we can calculate the minimum error for $\frac{\Delta\beta}{\beta}$, i.e.,

$$\frac{\Delta\beta}{\beta} = \frac{y - (3.01)y}{(3.01)y} \frac{\Delta C}{(1.10)},$$

or

$$\frac{\Delta\beta}{\beta} = -(0.607)\frac{\Delta C}{C}.$$

For the MILL RACE data analysis, the measurement error ΔC was approximately 0.02*

From Eqn. (3-21) and for $C_o \simeq 0.7$, we find the minimum error in C occurs for

$$C = .258 \tag{3-22}$$

Therefore, we find the minimum error in the deduced attenuation coefficient to be:

$$\frac{\Delta\beta}{\beta} = -(.047),$$

or about 5%.

Based on the results shown in Eqns. (3-15) and (3-22), we have derived the following guidelines in analyzing the MILL RACE data:

      1. Apparent Contrast C

$$0.1 \leq C \leq 0.5$$

      2. Apparent Contrast Ratio

$$0.5 \leq \ln C_i - \ln C_j \leq 1.50.$$

During data analysis, these rules were observed when possible. For some cases, the rules were violated because of a lack of data; these cases are identified.

* This error was due to the reading resolution of the densitometer used to measure contrast from the MILL RACE films.

52

3.4   DETERMINATION OF THE CONTRAST ATTENUATION COEFFICIENT

Equation (3-7) can be rewritten as follows:

$$\beta = \frac{1}{R_j - R_i} \ell n \frac{C_i}{C_j} \cdot \tag{3-7}$$

Applying the selection rules defined in the previous section to the contrast data, we deduced values for β at both the 10 psi and 20 psi station for intervals of one second after shock arrival until 40 seconds and at five second intervals from 40 seconds until 60 seconds. The results are shown in Table (3-2) and consist of an average and standard deviation for β when more than one pair of targets meets the selection rule guidelines.

All of the data shown in Table (3-2) were obtained from the Flight Research 35mm data films by using the diffuse densitometry measurements. In addition, we made measurements on several selected frames of the GSAP 16mm data film at the 10 psi station using the microdensitometer. The results are shown for several different times in Table (3-3). Although the agreement is not exact, the differences can be explained by considering the methods used to deduce contrast of a photo-target with the diffuse densitometer and the microdensitometer.

Figure (3-8) depicts a photo-target being analyzed by both instruments. In the top diagram, we see that the densitometer beam covers over one half the image of the photo-target and a similar area for the background measurement. Thus, the measured film contrast is deduced by averaging over a relatively large area. Any small dust inhomogeneities will be smoothed out.

On the other hand, the bottom half of Fig. (3-8) shows the size of the microdensitometer beam on the film. Note that the beam size (.071mm dia) is less than 1/14 the size of a photo-target. By slightly displacing the position of the beam, it was possible to change the measurement of the film's density by substantial amounts. In particular, the background measurement was highly sensitive to the vertical location of the densitometer's beam and by moving the beam one mm on the 16mm frame, it was possible to change the contrast reading by about 50%. Obviously, with that sensitivity, it would not be possible to expect exact agreement between these different measurements.

As an additional check between the measurements obtained by using either the diffuse or the microdensitometer, we performed the following procedure. Several Flight Research film frames were scanned with the micro-densitometer over the two targets and backgrounds. Since we previously obtained data from these films with the diffuse densitometer, a direct comparison between the two different densitometers on the same film was now possible. The results are shown in Table (3-4). Again we see that exact agreement does not occur and again we attribute the differences to the size of the beam used to scan the films in the densitometer. By using the difference in β measured by the microdensitometer as compared to the diffuse densitometer, we calculated the required change in background film density necessary to produce this difference; the results ranged between (5-8)%. Since a typical data frame had a background film density that changed by over a factor of two when scanned vertically by the micro-densitometer, a change of even 10% would not be unreasonable for small changes in the scanned position.

Table 3-2). Attenuation coefficients, β, for both the 10 psi and 20 psi station at MILL RACE as deduced from the Contrast Attenuation Technique.

Time (sec)	$\beta@10$ psi m^{-1}	(standard deviation)	$\beta@20$ psi m^{-1}	(standard deviation)
7	.24*		--	
8	.35		--	
9	.36		--	
10	.32	(.04)	--	
11	.29	(.02)	--	
12	.27	(.04)	--	
13	.24	(.06)	--	
14	.30	(.03)	--	
15	.27	(.05)	--	
16	.22	(.02)	.39	(.073)
17	.24	(.05)	.41	(.145)
18	.22	(.05)	.60	(.46)
19	.19	(.03)	--	--
20	.15	(.02)	--	--
21	.16	(.05)	--	--
22	.24	(.01)	.41	(.067)
23	.18	(.001)	.43	(.045)
24	.19	(.009)	.41	(.041)
25	.13	(.045)	.44	(.125)
26	.11	(.035)	.47	(.115)
27	.11	(.042)	.43	(.085)
28	.077	(.036)	.40	(.098)
29	.053	(.011)	.22	(.19)
30	.067	(.005)	.04	(.023)
31	.083	(.016)	.081*	(.054)
32	.063	(.008)	.12*	--
33	.065	(.020)	.078*	--
34	.056	(.010)	.088*	(.048)

Table 3-2 (Continued)

Time (sec)	$\beta@10$ psi m^{-1}	(standard deviation)	$\beta@20$ psi m^{-1}	(standard deviation)
35	.045	(.004)	.17	(.087)
36	.041	(.003)	.16	(.114)
37	.047	(.005)	--	--
38	.067	(.008)	.086	--
40	.056	(.012)	.11	--
45	.055	(.008)	.080*	(.040)
50	.037	(.006)	.024*	--
55	.048	--	.014*	--
60	.030	--	.015*	--

* These values do not conform to the selection rules given in Section 3.3.1 and therefore used with discretion.

Table (3-3). Attenuation Coefficients for the Flight Research 35mm camera and the GSAP 16mm camera at 10 psi and at several different times after shock arrival.

Time (sec)	β - Flight Research (m^{-1})	β - GSAP (m^{-1})
11	.29	.24
14	.30	.19
17	.24	.15

Table (3-4). Attenuation coefficient for the 10 psi Flight Research camera at several different times as measured by the diffuse and micro-densitometer.

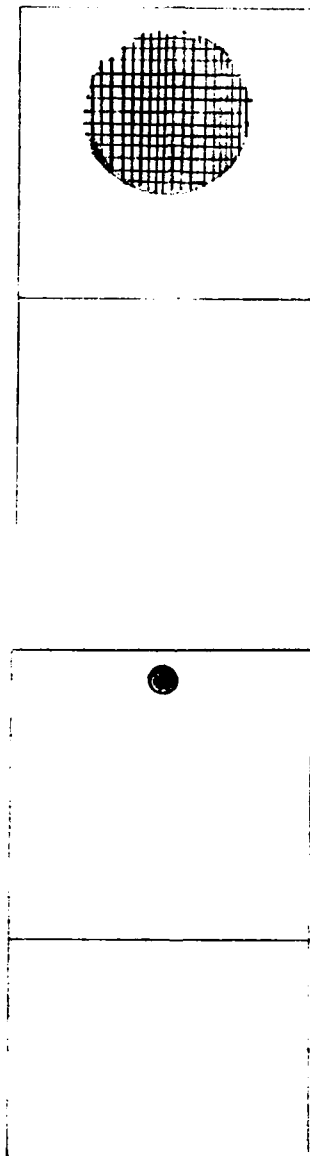| Time (sec)	β- Diffuse Densitometer (m^{-1})	β- Microdensitometer (m^{-1})
11	0.29	0.43
14	0.30	0.36
28	0.55	0.47

Figure (3-8)   Schematic of photo target's image and densitometer beam size.
The top figure depicts the diffuse densitometer while the
bottom figure depicts the microdensitometer.

SECTION 4

DETERMINATION OF DUST DENSITIES

In Section 3 we determined values for the attenuation coefficient, β, from the MILL RACE film data; these data are shown in Table 3-1. From Eqn. (1-1) (repeated below) in order to determine dust densities, we need values for the grain density, ρ_g, and the term enclosed within the brackets.

$$\rho_m = \frac{4}{3} \rho_g \beta \left[\frac{\int_{a_{min}}^{a_{max}} a^3 f(a) da}{\int_{a_{min}}^{a_{max}} Q(a) a^2 f(a) da} \right]. \tag{1-1}$$

A sample of dust from the MILL RACE CAT test area was analyzed by members of the Atmospheric Science Laboratory at WSMR. They provided a value for ρ_g and also values for the refractive index of the dust; these are given below.

$$\rho_g = 2.3 \text{ g/cm}^3 \tag{4-1}$$

$$n = (1.54) - i(2 \times 10^{-3}), \tag{4-2}$$

where $i = \sqrt{-1}$.

In Appendix B, the rationale for choosing Q_{ext} instead of Q_{sc} for use in Eqn. (1-1) is given. Fig. (4-1) shows the calculated values of Q_{ext} that were based on Mie theory, the refractive index given in Eqn. (4-2), and at a wavelength of $\lambda = 0.55$; this Q_{ext} was used for calculating the term inside the brackets of Eqn.(1-1).

The expression for $f(a)da$ has to be determined from the MILL RACE test site and should be measured at each interval of time corresponding to our film data. A separate experiment, fielded by SAI with the assistance of the U.S. Army's Atmospheric Sciences Lab, was tasked to make these measurements. A separate Report in these Proceedings describe the SAI experiment. For our needs, only the time-resolved particle size distribution function was necessary to deduce dust densities using Eqn. (1-1). However, SAI (Dr. John Cockayne) volunteered to compute the entire
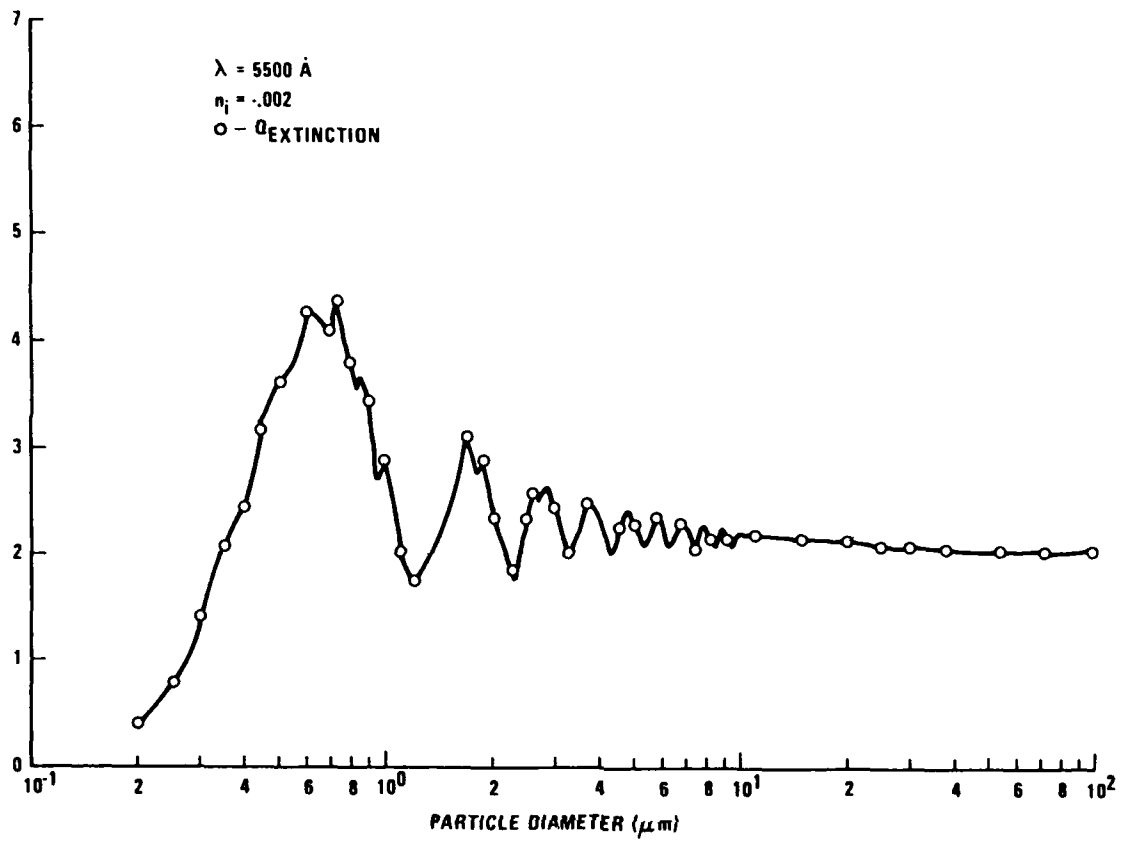
59

Fig.(4-1) Calculated value of Q_{ext} using Mie theory at $\lambda=0.55\mu$ and for WSMR dust.

expression within the brackets using our values for $Q(a)$ and a previously supplied computer code along with their measured values of $f(a)da$. This was done and the results are shown in Table (4-1) for the 10 psi station.

Given the data of Table (4-1), we can now compute absolute dust density vs time spectra for the 10 psi station using Eqn. (1-1). The results of such a calculation are provided in Table (4-2) (where the average of the two measurements at the 10 psi station was used). The corresponding values of dust density as measured by SAI are shown along side our CAT deduced data. The ratio of these dust densities deduced from the two different methods is given in Table (4-3). Averaging of the entries produces the following:

$$@ \ 10 \ psi \ \left[\frac{\rho_m \ (CAT)}{\rho_m \ (meas)} \right]_{Average} = 2.40 \text{ with a standard deviation of } 0.61$$

Referring to the measured data of Table (4-1) provided by SAI, the two measurement instruments at the 10 psi station were significantly different in their readings; over the same time interval shown in Table (4-2), the two measured values of ρ_m differed by an average factor of 1.67 with a standard deviation of 0.62, i.e.,

$$@ \ 10 \ psi \ \left[\frac{\rho_m(meas \ \#1)}{\rho_m(meas \ \#2)} \right]_{Average} = 1.67 \text{ with a standard deviation of } 0.62$$

If in fact the dust density changed by a factor of 1.7 between two measuring instruments separated by only 15 meters, it is very likely that our CAT-deduced dust density, which is a path-averaged value over a path-length up to 45 meters, would also show a substantial difference. Thus, given that the measured values for the dust density are correct, it would not be unreasonable to expect a factor of 2.4 between the CAT-deduced and measured dust density.

61

Table (4-1)   Calculated values of the expression:

$$\frac{4}{3}\left[\frac{\int_{a_{min}}^{a_{max}}a^3f(a)\,da}{\int_{a_{min}}^{a_{max}}Q(a)a^2f(a)\,da}\right]$$

supplied by SAI for the 10 psi test station.
Note that two different measurements were
obtained at the 10 psi station.

Time (sec)	10 psi station	
	#1 (microns)	#2 (microns)
1	1.96	2.13
2	7.68	8.14
3	7.28	8.01
4	9.42	7.39
5	9.48	7.40
6	7.26	8.84
7	7.25	8.82
8	6.75	7.34
9	6.74	7.33
10	6.11	8.20
11	6.13	8.16
12	5.33	5.35
13	5.30	5.14
14	5.27	5.21
15	5.18	5.33
16	5.20	5.08
17	5.17	5.04
18	5.01	4.84
19	4.99	4.77
20	4.91	4.52
21	4.90	4.44
22	4.76	4.23
23	4.75	4.32
24	4.67	4.46
25	4.73	4.25
26	4.83	3.90
27	4.77	3.92
28	3.49	3.46
29	3.32	3.40
30	3.55	3.33

Table (4-1) Continued

Time (sec)	10 psi station	
	#1 (microns)	#2 (microns)
31	3.52	3.33
32	3.18	2.99
33	3.22	2.97
24	3.50	2.99
35	3.25	2.94
36	2.95	2.98
37	2.96	2.97
38	3.56	2.82
39	3.56	2.77
40	3.49	3.22
41	3.50	3.28
42	3.72	3.54
43	3.90	3.53
44	3.07	3.35
45	2.96	3.35
46	2.57	3.17
47	2.60	3.13
48	3.60	3.77
49	3.74	3.98
50	3.75	3.24
51	3.55	3.26
52	3.31	3.19
53	3.60	3.13
54	3.20	2.51
55	3.00	2.47
56	3.20	3.15
57	3.29	3.11
58	2.24	2.56
59	2.33	2.54
60	2.18	2.49

Table (4-2) CAT deduced dust densities vs time and measured values of dust densities vs time provided by SAI

Dust Density ($10^{-6} g/cm^3$)

Time (sec)	10 psi station	
	CAT	MEASURED
7	5.91	4.92
8	7.56	2.87
9	7.77	2.88
10	7.02	3.91
11	6.35	3.91
12	4.42	1.39
13	3.84	1.42
14	4.82	1.56
15	4.35	1.55
16	3.47	1.31
17	3.76	1.32
18	3.32	1.17
19	2.84	1.19
20	2.17	1.06
21	2.29	1.07
22	3.31	0.81
23	2.50	0.80
24	2.66	0.71
25	1.79	0.71
26	1.47	0.55
27	1.47	0.54
28	0.82	0.33
29	0.55	0.34
30	0.71	0.33
31	0.87	0.33
32	0.60	0.25
33	0.62	0.22
34	0.56	0.23
35	0.43	0.26
36	0.37	0.25
37	0.43	0.25
38	0.66	0.26
..	....	....
40	0.58	0.30
45	0.53	0.27
50	0.40	0.22
55	0.40	0.17
60	0.21	0.13

64

Table (4-3)   Ratio of CAT-deduced dust density to measured values of dust density vs time

Time (sec)	$\rho_m(CAT)/\rho_m$ (meas) 10 psi static
7	1.20
8	2.63
9	2.70
10	1.80
11	1.62
12	3.18
13	2.70
14	3.09
15	2.81
16	2.65
17	2.85
18	2.84
19	2.39
20	2.05
21	2.14
22	3.85
23	3.13
24	3.75
25	2.52
26	2.67
27	2.72
28	2.48
29	1.62
30	2.15
31	2.64
32	2.40
33	2.82
34	2.43
35	1.65
36	1.48
37	1.72
38	2.54
..	....
..	....
40	1.93
45	1.96
50	1.82
55	2.35
60	1.62

SECTION 5
CONCLUSIONS

The results of the MILL RACE validation experiment of the CAT method for deducing dust densities indicate that this method produced a value greater than the measured dust density by a factor of 2.4 ± 0.61. By using reasonable, conservative arguments we believe that the CAT method produces dust densities to within a factor of about two of the actual path-averaged values.

68

BIBLIOGRAPHY

Snow, R., M. L. Price and J. P. Doty, "Determination of Shock-Entrained Dust Concentration from Photographic Records of Nuclear Weapon Tests," DNA 5119F, Teledyne Brown Engineering, June 1980.

McCartney, E. J., "Optics of the Atmosphere," John Wiley & Sons, 1976.

Plass, G. N., "Mie Scattering and Absorption Cross Sections for Absorbing Particles," Applied Optics, Vol. 5, No. 2, p. 279, Feb. 1966.

Middleton, W.E.K., "Vision Through the Atmosphere," University of Toronto Press, 1952.

Douglas, C. A. and R. L. Booker, "Visual Range," NBS Monograph 159, 1977.

APPENDIX A

THEORETICAL DERIVATION OF CONTRAST ATTENUATION
TECHNIQUE EQUATIONS

Consider a diffuse target, T, located at distance R from an observation point, O (see Fig. A-1). Let Ω be the solid angle at O subtended by T along the path r.

The irradiance, E, at O produced by the target is given by

$$E(T) = \frac{I(T)\Omega}{\pi} \exp(-\beta_{ex}R) \tag{A-1}$$

where β_{ex} is the extinction coefficient along r (assumed constant) and I (T) is the radiance of T. For visible radiation and a non-emitting target:

$$I(T) = \rho H(R,t) \tag{A-2}$$

where ρ is the reflectivity of T and H (R,t) is the visible irradiance of T at time t due to all causes (sun, scattered light, etc.). Thus,

$$E(T) = \rho \frac{H(R,t) \ \Omega}{\pi} \exp(-\beta_{ex}R) . \tag{A-3}$$

A second source of visible irradiation of O arriving within Ω is the so-called "Airlight" or path radiance which is the total light scattered into the field of view of O along r from all sources including the sun, sky and terrain. The airlight irradiation at O can be found by the following expression:

$$E(A) = \int_0^R H(r,t) \ \beta_{sc} \exp(- \beta_{ex}r) \ dr, \tag{A-4}$$

where β_{sc} is the scattering coefficient towards O. For the case when β_{ext}, H(r,t) and β_{sc} are all constant along r, we can integrate (A-4) to find:

$$E(A) = \frac{H(t) \ \beta_{sc}}{\beta_{ex}} [1-\exp(-\beta_{ex}R)]. \tag{A-5}$$

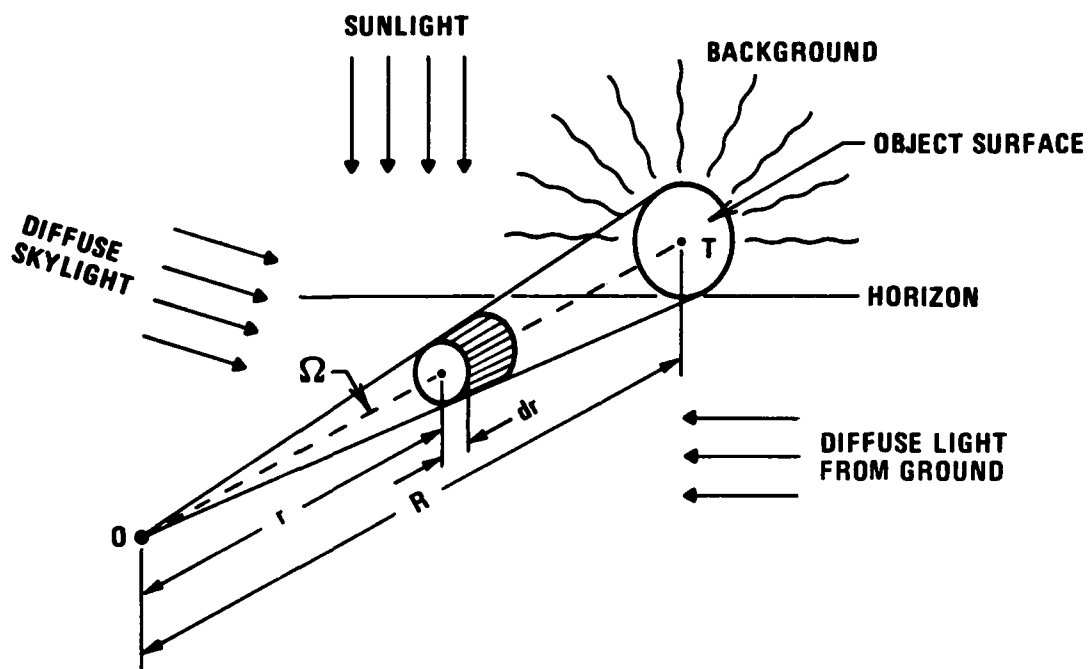The sum of (A-3) and (A-5) describe the total irradiance at O arriving within the angle Ω:

Fig.(A-1)   Source of the airlight between the observer at 0 and an
object at R.   (From <u>Optics of the Atmosphere</u>, E.J. McCartney, John
Wiley & Sons, 1976, p. 35).

$$E(R) = E(T) + E(A) = \frac{\rho H(R,t)\Omega}{\pi} \exp(-\beta_{ex}R)$$

$$+ \frac{H(t) \ \beta_{sc}}{\beta_{ex}} [1-\exp(-\beta_{ex}R)]. \tag{A-6}$$

Note that $H(R,t)$ is not equal to $H(t) = H(r,t)$ when $r \neq R$ because the target itself blocks radiation from portions of the surroundings at T.

The irradiance at 0 produced by the background just outside of Ω is found from Eqn. (A-4) with the limits of integration extending to infinity, viz.,

$$E(B) = \int_0^\infty H(r,t) \ \beta_{sc} \ \exp \ (-\beta_{ex}r) \ dr$$

or when $H(r,t,) = H(t)$,

$$E(B) = \frac{H(T)\beta_{sc}}{\beta_{ex}} . \tag{A-7}$$

Equation (A-7) applies when the background radiance is not due to any specific feature such as a hill, tree, etc., but due only to airlight extending into the sky towards the horizon.

Visibility of the target at 0 occurs when the contrast between the target and its background exceeds a threshold which depends on the detecting element. Contrast, C, is defined by:

$$C = \frac{E(R) - E(B)}{E(B)} , \tag{A-8}$$

or,

$$C = \frac{\rho H(R,t)\frac{\Omega}{\pi}\beta_{ex} - H(t)\beta_{sc}}{H(t) \ \beta_{sc}} \ \exp(-\beta_{ex}R). \tag{A-9}$$

The inherent contrast of a target, C_o, is found by letting the observer at 0 approach the target, i.e., letting $R \to 0$. Reviewing Eqns. (A-1) to (A-8), this produces the following expression:

$$C_o(T) = \frac{\rho H(R,t)\frac{\Omega}{\pi} \ \beta_{ex} - H(t) \ \beta_{sc}}{H(t) \ \beta_{sc}} \tag{A10}$$

or combining Eqns. (A-9) and (A-10), we find:

$$C(t) = C_o(t) \exp(- \beta_{ex} R),$$ (A-11)

which is commonly referred to as "Koschmeider's Law", although Duntley and others contributed to its derivation.

An explicit assumption for the derivation of Eqn. (A-11) is the uniformity of the intervening medium between the target and the observer. This allows the use of a single extinction and scattering coefficient, β_{ex} and β_{sc}, to be used. In principle one could derive a similar expression with non-uniform β_{ex} and β_{sc}; in this case one would have to know their properties and perform several additional integrations along the path r. We assume that an average value of β_{ex} and β_{sc} exists and satisfies Eqns. (A-1) to (A-11).

A serious limitation on using Eqn. (A-11) to find β_{ex} for a time-varying case such as MILL RACE was the necessity of defining both $C(t)$ and $C_o(t)$ at the same time, t. For cases when $C_o(t)$ is constant or well defined, one can use pre-determined measurements and/or calculations for $C_o(t)$ along with the measured value of $C(t)$ and thus solve Eqn. (A-11) for β_{ex}. Unfortunately, during the MILL RACE experiment neither case applied, i.e., conditions surrounding the target/camera path length were rapidly changing in time. This situation affects the values of $H(R,t)$, $H(t)$, and also values for β_{ex} and β_{sc}. An alternative method can be used if the following conditions existed:

1. Measurements were made of multiple targets at the same time.

2. The intervening medium was uniform.

3. The inherent contrast of the targets were all equal.

If such conditions existed, then we can write an Eqn. (A-11) for each independent target, i.e.,

$$C_1(t) = C_o(t) \exp(-\beta_{ex} R_1),$$

$$C_2(t) = C_o(t) \exp(-\beta_{ex} R_2),$$

etc. Dividing these two Eqns., we can write,

$$\frac{C_1(t)}{C_2(t)} = \exp(-\beta_{ex}[R_1 - R_2]),$$ (A-12)

and since $(R_1 - R_2)$ was a known value while $C_1(t)$ and $C_2(t)$ were measured at 0, we can solve Eqn. (A-12) for β_{ex} viz.,

$$\beta_{ex}(t) = \frac{\ell n \left[\dfrac{C_1(t)}{C_2(t)}\right]}{R_2 - R_1} \; . \tag{A-13}$$

Of course, for (n) targets we can solve Eqn. (A-12) for (n-1) values of β_{ex}, viz.,

$$\beta_{ex}(t) = \frac{\ell n \left[\dfrac{C_i(t)}{C_{i+1}(t)}\right]}{R_{i+1} - R_i} \quad , \quad i = 1, 2, \ldots, n-1. \tag{A-14}$$

Once we solve for β_{ex}, the value of $C_o(t)$ can also be found from Eqn. (A-11). By iterating this technique for many different times and for many different targets, it becomes possible to begin a systematic study of the time dependent behavior of β_{ex}.

APPENDIX B

MIE SCATTERING AND EXTINCTION CONSIDERATIONS

Contrast attenuation of visible radiation in the atmosphere occurs according to Koschmeider's Eqn.:

$$C_R = C_o \exp(-\beta R), \qquad (B-1)$$

where C_R, C_o are the apparent contrast at distance R and inherent contrast, respectively, while β refers to the attenuation coefficient for either scattering (β_{scat}) or extinction (β_{ext}). Since the basis of the CAT to deduce dust densities depends upon the definition of β, we undertook a sensitivity study to determine the best choice of β and the effect of changing its value.

A brief review of elementary Mie scattering theory is necessary in order to discuss the pertinent factors. Recall that Mie theory applies for all sizes of spherically shaped, isotropic particles at all wavelengths. Mie found that the parameter $\alpha = \dfrac{2\pi a}{\lambda}$ (where a is the particle radius and λ the wavelength) determines the distribution of phase over the particle; when $\alpha \ll 1$, Mie theory reduces to Rayleigh scattering while for $\alpha \gg 10$, the principles of diffraction, reflection and refraction adequately describe the particle's interaction with the radiation. In the midrange of relative particle size, however, the use of the full Mie theory becomes mandatory. For most of the sizes of dust particles encountered at MILL RACE, the full Mie theory applies.

The second vital parameter used for Mie scattering calculations is the index of refraction of the particle. When absorption is insignificant, only scattering occurs and the refractive index is expressed as a real number, n. When the particle is absorbing significantly, the refractive index must be expressed by a complex number, i.e.,

$$m = n - i n_i \ , \qquad (B-2)$$

where m is the refractive index with n and n_i the real and imaginary parts, respectively, and $i = \sqrt{-1}$. The imaginary part is related to the absorption coefficient of the particle.

Referring back to Koschmeider's Eqn., we can relate β_{scat} to the real index of refraction while β_{ext} obtains for the complex case. Once

77

the refractive index is specified, a calculation of the intensity distribution function for radiation interacting with the particles becomes tractable through the use of the Mie theory. The results are usually expressed in terms of an angular cross section, $\sigma(\Theta)$, for scattering by the particle, and defined as that cross section of an incident wave, acted on by the particle, having an area such that the power flowing across it is equal to the scattered power per steradian at an observation angle Θ. By integrating over all scattering angles, one can determine the total scattering cross section, defined as that cross section of the incident wave acted on by the particle, having an area such that the power flowing across it is equal to the total power scattered in all directions; or

$$\sigma = \int_{0}^{4\pi} \sigma(\Theta) d\omega \qquad (B-3)$$

A more useful parameter than σ is the efficiency factor Q, which can be defined for both scattering and extinction. Q_{sc} is defined as the ratio of the scattering cross section to the geometric cross section, i.e.,

$$Q_{sc} = \frac{\sigma}{\pi a^2}, \qquad (B-4)$$

while Q_{ext} is defined as

$$Q_{ext} = Q_{sc} + Q_{ab}, \qquad (B-5)$$

where Q_{ab} is the efficiency factor for absorption. Mie theory allows one to calculate both Q_{sc} and Q_{ext}; their difference equals Q_{ab}. We do not intend to discuss further the derivation of these parameters. We do intend to describe the differences resulting from including absorption in the CAT theory.

Figure (B-1) shows the effect of including absorption in the calculation of Q_{sc} for various values of Q_{ab}. Note that as absorption increases from $n_i \leq 10^{-4}$ to $n_i = 10^{-1}$, the limiting value of Q_{sc} as α becomes very large is between 1.00 and 1.11, increases to 1.2 when $n_i = 1$, and is near 1.95 when $n_i = 10$. The limiting value of Q_{ext} approaches two in all cases. It appears that the asymptotic values of both Q_{sc} and Q_{ext} approach two as Q_{ab} becomes larger, while for very small values of Q_{ab},

78

the limiting value for Q_{sc} goes to one while Q_{ext} continues towards two. Thus for very large particles and/or short wavelength cases, we need to use the extinction efficiency factor for calculating changes in contrast or else a serious error (on the order of e^2) may result.

The MILL RACE data pertains to dust particles with radius extending upwards of 30 microns. For visible light, this produces an $\alpha \sim 300$ which satisfies the "very large α" criteria. Thus we need to compute Q_{ext} for this case to determine its significance in calculating the contrast attenuation.

Values for the index of refraction for MILL RACE soil were measured by WSMR and found to be:

$$m = 1.54 - .002i$$

A calculation was made for both Q_{sc} and Q_{ext} at 260 different values of $d = 2a$, viz.,

$$\Delta d = 0.01\mu \quad \text{for } 0.2 \leq d \leq 1.0$$
$$\Delta d = 0.1\mu \quad \text{for } 1.0 \leq d \leq 10$$
$$\Delta d = 1.0\mu \quad \text{for } 10 \leq d \ 100,$$

and for different wavelengths,

$$\lambda = .40.42, \ \ldots \ ..68,.70,$$
$$\lambda = .55\mu$$
$$\text{and} \quad \lambda = .6328 \ \mu$$

(The latter wavelength was used in the PMS particle sizing instrument).
The results for Q_{sc} and Q_{ext} at $\lambda = .55$ are shown in Fig. (B-2). As expected, the asymptotic values diverge towards a factor of two difference, but the differences at small particle diameters ($d \leq 10\mu$) remain relatively close together. Fig.(B-3) shows the normalized difference between Q_{sc} and Q_{ext}.

The importance of the divergence between Q_{sc} and Q_{ext} depends on the relative weighting of these parameters caused by the particle size distribution function used to calculate β. The equation for β is the following:

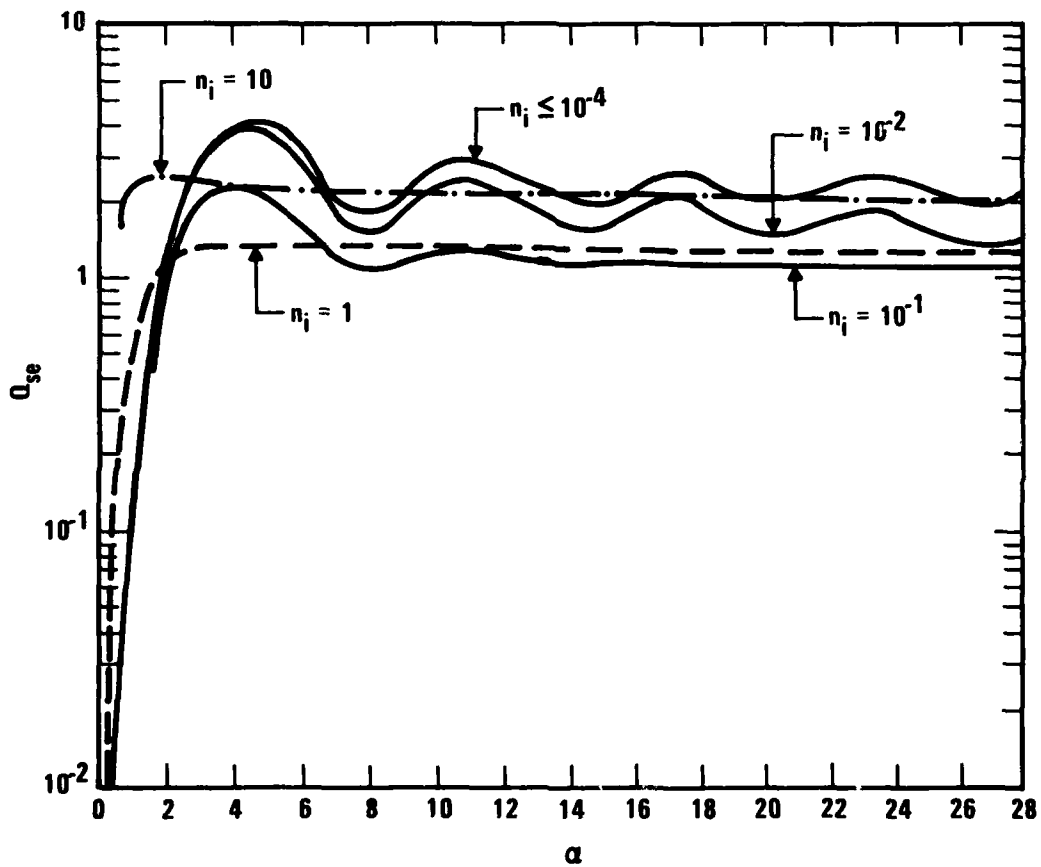$$\beta = \int_{a_{min}}^{a_{max}} \sigma \ N \ f(a) \ da, \tag{B-6}$$

79

Fig.(B-1) Efficiency factor for scattering as a function of $\alpha = \frac{2\pi a}{\lambda}$ and for several different values of the imaginary component of the refractive index n_i. The real component of the refractive index is constant and equal to 1.5. (From Appl. Opt. $\underline{5}$, No. 2 February 1966 p. 281).
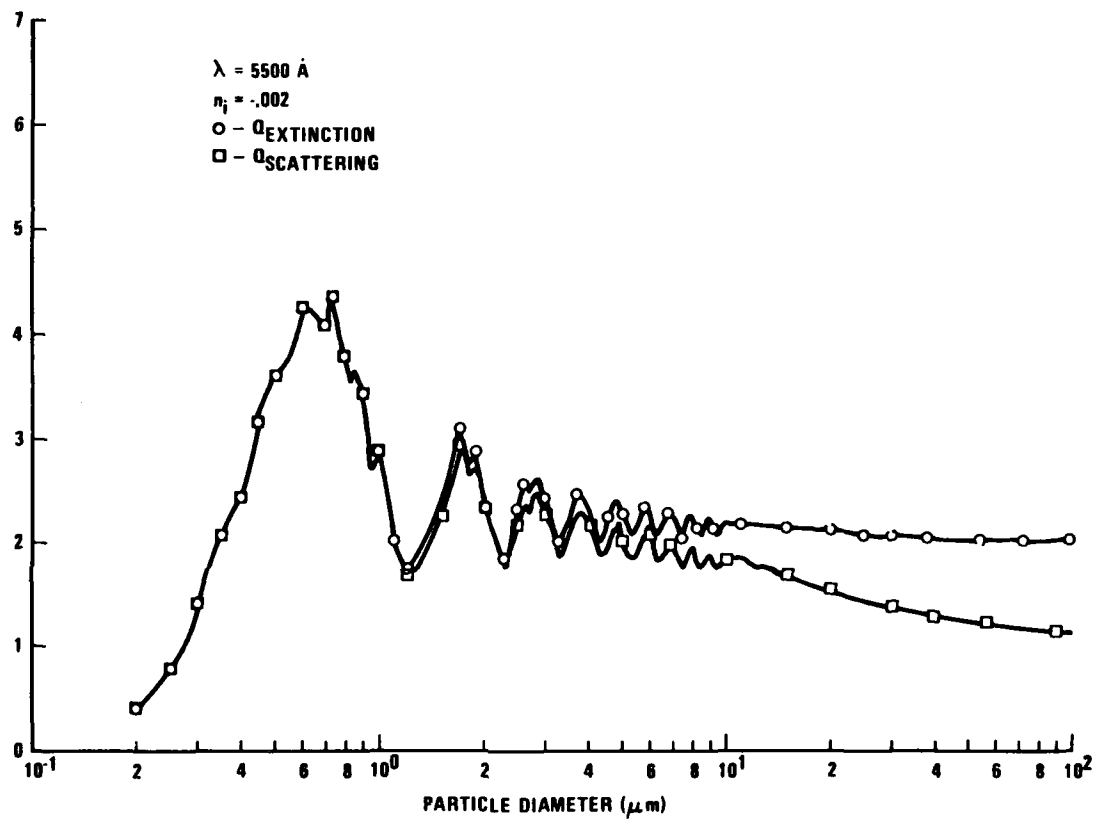
Fig.(B-2) Calculated values of Q_{sc} and Q_{ext} vs particle diameter for $\lambda=0.55\mu$ and for WSMR dust.
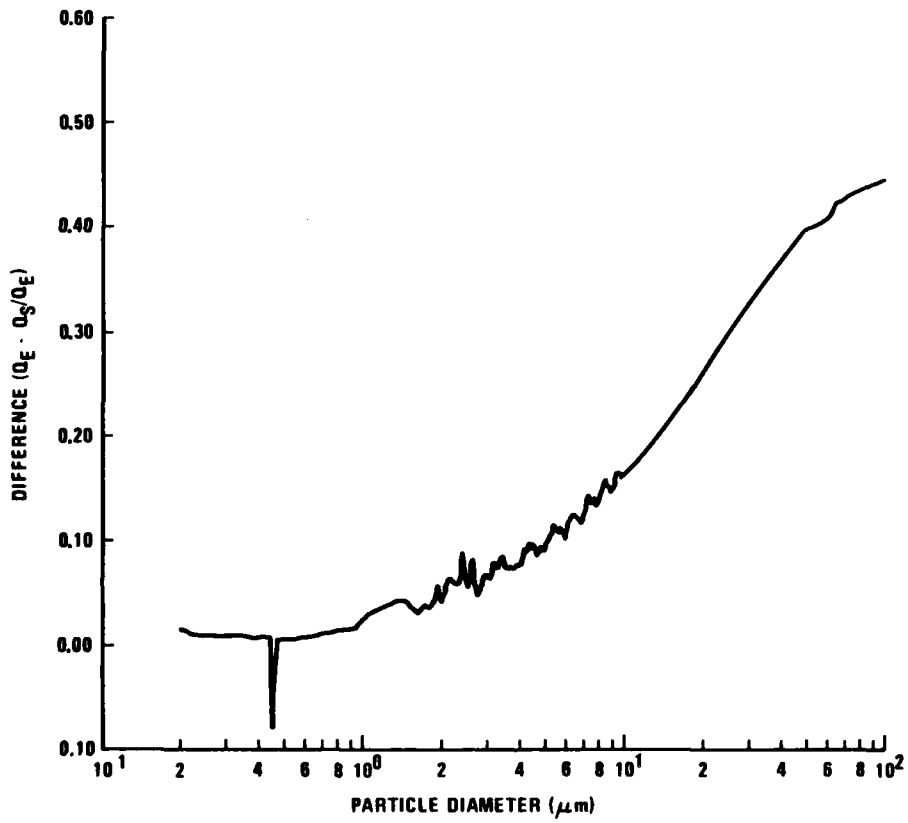
Fig.(B-3) Normalized difference between Q_{sc} and Q_{ext} as a function of particle diameter.

where N is the total particle concentration, $f(a)da$ is the fraction of particles having radius between a and $(a + da)$ and a_{max}, a_{min} are the maximum and minimum size particles contributing to the attenuation. We can rewrite Eqn. (B-6) as:

$$\beta = \pi \int_{a_{min}}^{a_{max}} a^2 QNf(a)da. \tag{B-7}$$

We see that the effect of changing Q from Q_{sc} to Q_{ext} depends on the second moment of the distribution function. Likewise the determination of ρ_m, the dust mass concentration is found from Eqn. (B-8):

$$\rho_m = \frac{4}{3} \rho_g \beta \left[\frac{\int_{a_{min}}^{a_{max}} a^3 f(a)da}{\int_{a_{min}}^{a_{max}} a^2 QF(a)da} \right], \tag{B-8}$$

where σ_g is the grain density, and the other terms have already been defined. We have previously shown that an experimental determination of β can be found, e.g.,

$$\beta = \frac{\ln\left(\dfrac{C_1}{C_2}\right)}{R_2 - R_1}, \tag{B-9}$$

so that the derived value for ρ_m also depends on the value of Q in a comlicated way.

APPENDIX C

SELECTED DATA ON FILMS USED FOR
THE MILL RACE CAT VALIDATION TEST

KODAK HIGH DEFINITION AERIAL FILM 3414
(ESTAR THIN BASE)

This is an extremely fine-grain, slow speed, panchromatic, negative aerial camera film.
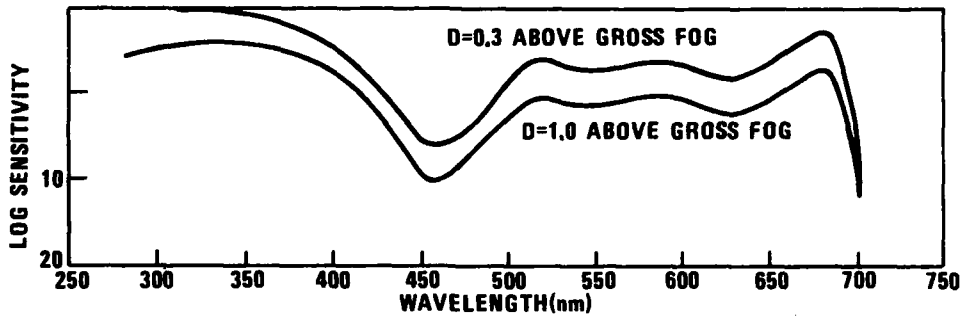
BASE: A 2.5mil (64 micrometer) Estar Thin Base
                with a B2 (dyed-gel) backing

SENSITIVITY: Panchromatic, with extended red sensitivity

AERIAL EXPOSURE INDEX: Daylight (no filter) - 2.5*

AERIAL FILM SPEED: Daylight (no filter) - 8.0*

RMS GRANULARITY VALUE: 9 (at a net density of 1.0)*

RESOLVING POWER: Test-Object Contrast 1000:1-630
                                                        lines/mm*

                                    Test-Object Contrast 1.6:1-250
                                                        lines/mm*

*These data are based on development in Kodak developer D-19 at 66F for
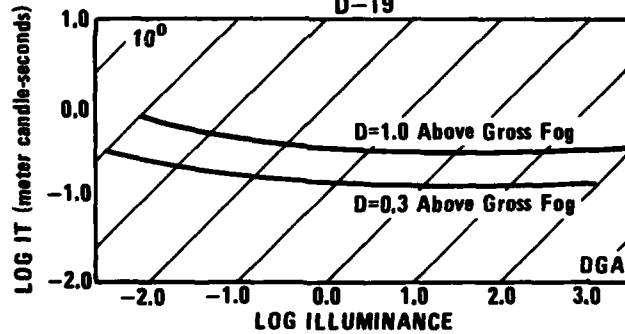8 minutes in a sensitometric processing machine.

SPECTRAL SENSITIVITY CURVES
D-19

MODULATION-TRANSFER CURVES
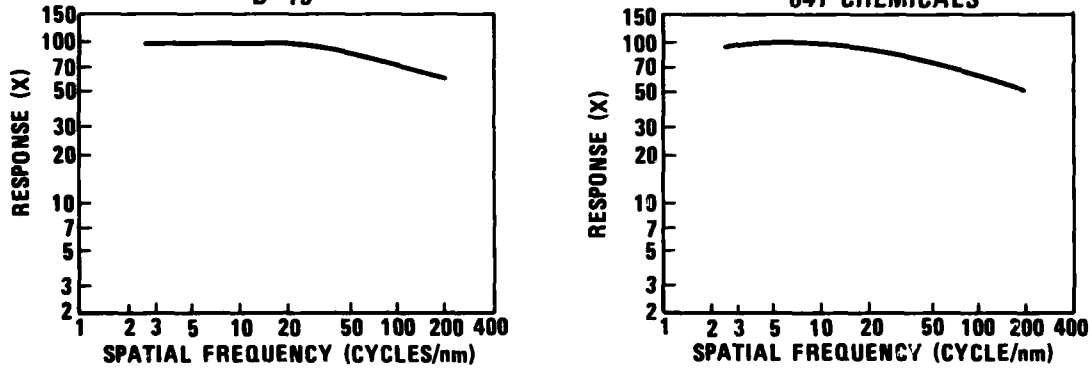
RECIPROCITY CURVES
D-19

CHARACTERISTIC CURVES
641 CHEMICALS
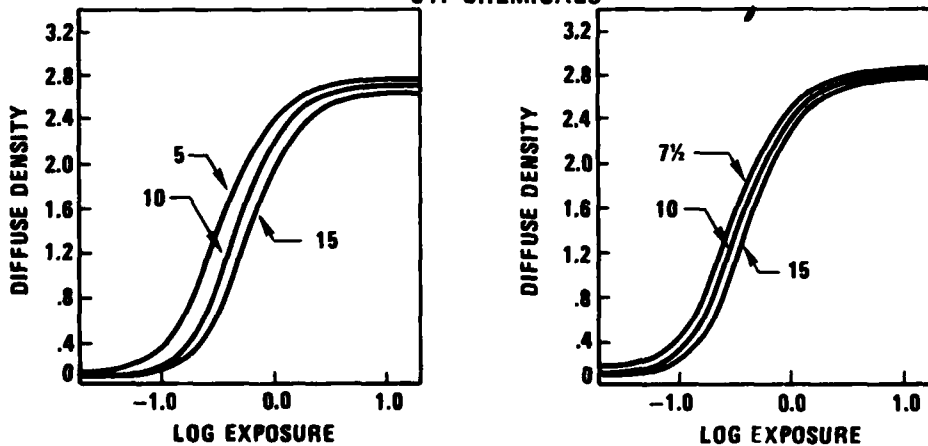
Fig. (C-1)   Data for Kodak 3414 High Definition Aerial Film.

87

KODAK LINAGRAPH SHELLBURST FILM 2476
(ESTAR AH-BASE)

This is a medium grain, medium speed, panchromatic, high resolution, negative film.

BASE: A .004 inch (102 micrometer) ESTAR-AH base with a fast-drying backing

SENSITIVITY: Panchromatic with extended red sensitivity

EXPOSURE INDEX: 250*

DIFFUSE RMS GRANULARITY VALUE: 22*

RESOLVING POWER: Test-Object Contrast 1000:1-160 lines/mm*

Test-Object Contrast 1.6:1-63 lines/mm*

*Based on development in Kodak developer D-19 at 68F for 12 minutes using continuous agitation.

88

CHARACTERISTIC CURVES

KODAK LINAGRAPH
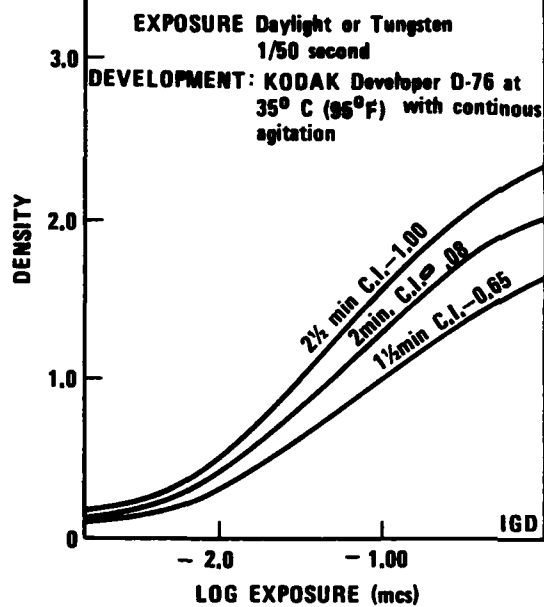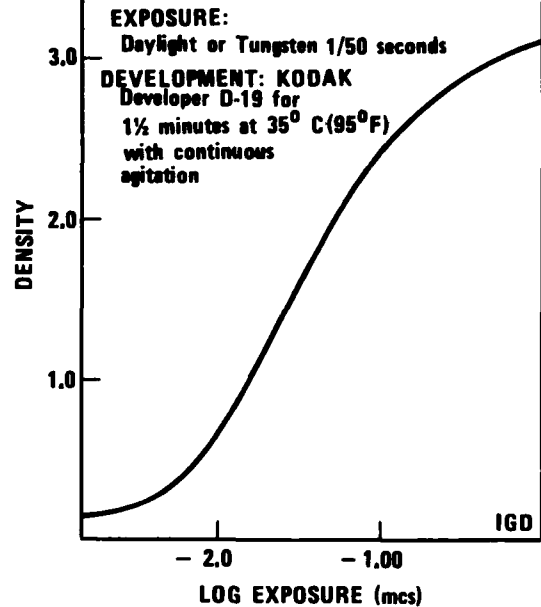**SHELLBURST FILM 2476 (ESTAR AH BASE)**

EXPOSURE Daylight or Tungsten
1/50 second
DEVELOPMENT: KODAK Developer D-76 at
35° C (95°F) with continous
agitation

2½ min C.I.-1.00
2min. C.I.-.08
1½min C.I.-0.65

DENSITY

LOG EXPOSURE (mcs)

IGD

CHARACTERISTIC CURVES

KODAK LINAGRAPH
SHELLBURST FILM 2476 (ESTAR AH BASE)

EXPOSURE:
Daylight or Tungsten 1/50 seconds
DEVELOPMENT: KODAK
Developer D-19 for
1½ minutes at 35° C(95°F)
with continuous
agitation

DENSITY

LOG EXPOSURE (mcs)

IGD

SPECTRAL SENSITIVITY CURVES

KODAK LINAGRAPH
SHELLBURST Film 2476 (ESTAR AH Base)

LOG SENSITIVITY
Reciprocal of exposure in ergs/cm² required to produce the densities given

D-0 30 Above Gross Fog

D-1.00 Above Gross Fog

Developed in KODAK Developer D-19 for
1½ minutes at 35°C (95°F) with
continuous agitation

WAVELENGTH (nm)
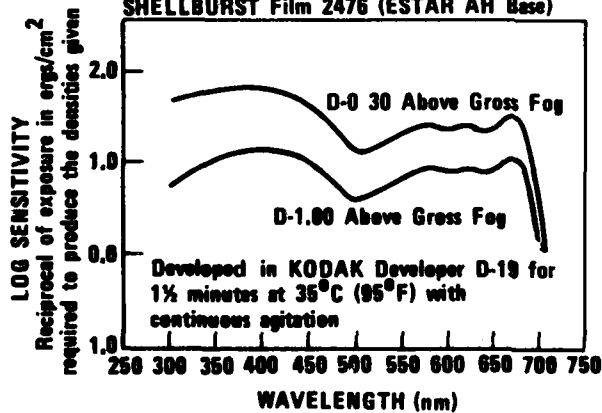
MODULATION TRANSFER CURVES

KODAK LINAGRAPH
SHELLBURST Film 2476 (ESTAR AH Base)

RESPONSE(%)

Developed in KODAK Developer D-19 for 1½
minutes at 35°C (95°F) with continuous
agitation

SPATIAL FREQUENCY (Cycles/mm)

Fig. (C-2)   Data for Kodak 2476 Linagraph Shellburst film.

89

90

DISTRIBUTION LIST

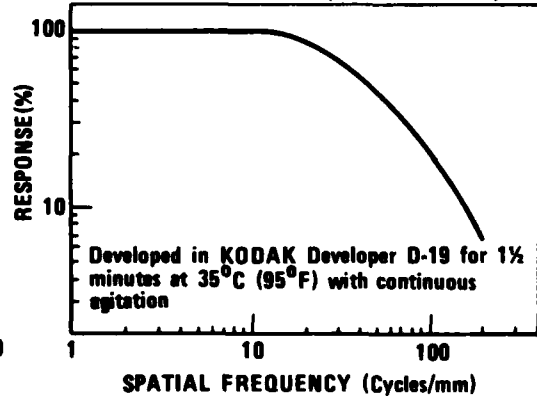DEPARTMENT OF DEFENSE

Assistant to the Secretary of Defense
Atomic Energy
    ATTN: Executive Assistant

Defense Communications Agency
    ATTN: CCTC

Defense Intelligence Agency
    ATTN: DT-2, T. Dorr
    ATTN: DB-4D
    ATTN: DT-1C
    ATTN: DT-2

Defense Nuclear Agency
    ATTN: SPTD
    ATTN: NATA
    ATTN: SPSS
    ATTN: STNA
    ATTN: STSP
3 cy ATTN: SPAS
4 cy ATTN: TITL

Defense Tech Info Center
12 cy ATTN: DD

Field Command
DNA Det 1
Lawrence Livermore Lab
    ATTN: FC-1

Field Command
Defense Nuclear Agency
    ATTN: FCTT
    ATTN: FCTT, W. Summa
    ATTN: FCTX
    ATTN: FCTXE
    ATTN: FCPR
    ATTN: FCTOF
    ATTN: FCTT, G. Ganong

Joint Chiefs of Staff
    ATTN: SAGA/SSD
    ATTN: GD50, J-5 Force Plng & Prog Div
    ATTN: GD10, J-5 Nuc & Chem Div
    ATTN: SAGA/SFD

Joint Strat Tgt Planning Staff
    ATTN: JLA, Threat Applications Div
    ATTN: JPTM
    ATTN: JPST
    ATTN: JLTW-2

Under Secretary of Def for Rsch & Engrg
    ATTN: Engr Tech J Persh
    ATTN: Strat & Thtr Nuc Forces, B. Stephan
    ATTN: Strat & Space Sys, OS

DEPARTMENT OF THE ARMY

BMD Advanced Technology Center
    ATTN: ATC-T, M. Capps

BMD Systems Command
    ATTN: BMDSC-H, N. Hurst

DEPARTMENT OF THE ARMY (Continued)

Dep Ch of Staff for Ops & Plans
    ATTN: DAMO-NCZ

Dep Ch of Staff for Rsch Dev & Acq
    ATTN: DAMA-CSS-N

Harry Diamond Labs
    ATTN: DELHD-NW-P
    ATTN: DELHD-NW-P, J. Gwaltney
    ATTN: DELHD-TF

US Army Ballistic Research Labs
    ATTN: DRDAR-BLT, J. Keefer
    ATTN: DRDAR-BLV, R. Vitali
    ATTN: DRDAR-BL, R. Eichelberger
    ATTN: DRDAR-BLV, W. Schuman Jr
    ATTN: DRDAR-BLT, D. Menne
    ATTN: DRDAR-TSB-S

US Army Material & Mechanics Rsch Ctr
    ATTN: DRXMR-HH, J. Dignam

US Army Materiel Dev & Readiness Cmd
    ATTN: DRCDE-D, L. Flynn

US Army Nuc & Chemical Agency
    ATTN: Library

US Army Research Office
    ATTN: P. Rakdowski, Consultant

US Army TRADOC Sys Analysis Actvy
    ATTN: ATAA-TDC, R. Benson

USA Missile Command
    ATTN: DRSMI-RKP, W. Thomas
    ATTN: DRSMI-RHB, H. Greene
    ATTN: DRSMI-RH

DEPARTMENT OF THE NAVY

Naval Research Lab
    ATTN: Code 2627
    ATTN: Code 7908, A. Williams
    ATTN: Code 4773, G. Cooperstein

Naval Sea Systems Command
    ATTN: SEA-0352, M. Kinna

Naval Surface Weapons Center
    ATTN: Code K06, C. Lyons
    ATTN: Code R15, J. Petes
    ATTN: Code F31

Naval Weapons Evaluation Facility
    ATTN: Code 70, R. Tillery
    ATTN: Code 70, L. Oliver

Ofc of the Deputy Ch of Naval Ops
    ATTN: NOP 654, Strat Eval & Anal Br

Strat Systems Project Office
    ATTN: NSP-272
    ATTN: NSP-273
    ATTN: NSP-2722, F. Wimberly

DEPARTMENT OF THE AIR FORCE

Aeronautical Systems Div
    ATTN: ASD/ENFTV, D. Sorgen
2 cy ATTN: ASD/ENFTV, D. Ward

Air Force Geophysics Lab
    ATTN: LY, C. Touart

Air Force Rocket Propulsion Lab
    ATTN: LKLP, G. Beale

Air Force Systems Command
    ATTN: XRTO
    ATTN SDM

Air Force Tech Applications Ctr
    ATTN: TF

Air Force Weapons Lab
    ATTN: NTYV, A. Sharp
    ATTN: HO, W. Minge
    ATTN: NTYV
    ATTN: NTES
    ATTN: SUL
2 cy ATTN: NTO

Air Force Wright Aeronautical Lab
    ATTN: FIMG
    ATTN: FBAC, D. Roselius

Air Force Wright Aeronautical Lab
    ATTN: MBC, G. Schmidt

Air University Library
    ATTN: AUL-LSE

Arnold Engrg Dev Ctr,
    ATTN: AEDC, DOFOV

Air Force Systems Command
    ATTN: ENSN, W. Wilson
    ATTN: SYDT
    ATTN: EN
    ATTN: HQ Space Div/RST
    ATTN: ENMR
    ATTN: HQ Space Div/RSS
    ATTN: ENSN Blankinship

Deputy Chief of Staff
Research, Development, & Acq
    ATTN AFRDQI
    ATTN: AFRD

Foreign Technology Div
    ATTN: SDBS, J. Pumphrey
    ATTN: TQTD
    ATTN: SDBG

USAF HDQ, Directorate of Ops
    ATTN: AFXOOTS

Space Division
    ATTN: AFML

Strat Air Command
    ATTN: XPFS
    ATTN: XPQM
    ATTN: DOXT
    ATTN: XOBM

DEPARTMENT OF ENERGY

Department of Energy
    ATTN: OMA/RD&T

OTHER GOVERNMENT AGENCY

Central Intelligence Agency
    ATTN: OSWR/NED

NATO

NATO School, SHAPE
    ATTN: US Doc Officer

DEPARTMENT OF ENERGY CONTRACTORS

University of California
Lawrence Livermore National Lab
    ATTN: L-262, J. Knox
    ATTN: L-125, J. Keller
    ATTN: L-8, R. Andrews

Los Alamos National Lab
    ATTN: R. Thurston
    ATTN: MS670, T. Scolman
    ATTN: R. Selden
    ATTN: D. Kerr
    ATTN: MS F668, R. Dingus
    ATTN: J. Hopkins

Sandia National Lab
    ATTN: Org 7112, A. Chabai
    ATTN: M. Cowan

Sandia National Labs, Livermore
    ATTN: T. Cook
    ATTN: Library & Security Class Div
    ATTN: H. Norris

DEPARTMENT OF DEFENSE CONTRACTORS

ACUREX Corp
    ATTN: C. Nardo
    ATTN: C. Powars

Aerojet General Corp
    ATTN: R. Steele

Aerospace Corp
    ATTN: H. Blase
    ATTN: R. Crolius

Analytic Services, Inc, ANSER
    ATTN: J. Selig

APTEK, Inc
    ATTN: T. Meagher

AVCO Systems Division
    ATTN: J. Stevens
    ATTN: W. Reinecke
    ATTN: W. Broding
    ATTN: J. Gilmore
    ATTN: P. Grady
    ATTN: A . Pallone
    ATTN: Doc Con

Battelle Memorial Institute
    ATTN: E. Unger
    ATTN: M. Vanderlind

92

DEPARTMENT OF DEFENSE CONTRACTORS (Continued)

Boeing Aerospace Co
    ATTN: M/S 13-13, R. Dyrdahl

Boeing Co
    ATTN: M/S 41-52, M. Susman
    ATTN: W. Hammon
    ATTN: M/S 85/20, E. York
    ATTN: R. Holmes
    ATTN: M/S 41/10, J. Avery

Boeing Military Airplane Co
    ATTN: MS 75-74, D. Sawdy

California Research & Technology, Inc
    ATTN: K. Kreyenhagen
    ATTN: M. Rosenblatt

Calspan Corp
    ATTN: M. Holden
    ATTN: M. Dunn

Dupont Chemical Corp
    ATTN: F. Bailey

G. B. Laboratory, Inc
    ATTN: G. Burghart

General Electric Co
    ATTN: P. Cline
    ATTN: B. Maguire

General Research Corp
    ATTN: J. Mate

H-Tech Labs, Inc
    ATTN: B. Hartenbaum

Harold Rosenbaum Associates, Inc
    ATTN: G. Weber

Hercules, Inc
    ATTN: P. McAllister

Institute for Defense Analyses
    ATTN: Classified Library

Kaman AviDyne
    ATTN: R. Ruetenik
    ATTN: S. Criscione
    ATTN: N. Hobbs

Kaman Sciences Corp
    ATTN: J. Harper
    ATTN: J. Hoffman
    ATTN: F. Shelton
    ATTN: J. Keith

Kaman Science Corp
    ATTN: D. Sachs

Kaman Tempo
    ATTN: B. Gambill
    ATTN: DASIAC

Lockheed Missiles & Space Co, Inc
    ATTN: F. Borgardt

Lockheed Missiles & Space Co, Inc
    ATTN: R. Walz

DEPARTMENT OF DEFENSE CONTRACTORS (Continued)

Martin Marietta Denver Aerospace
    ATTN: E. Strauss

McDonnell Douglas Corp
    ATTN: P. Lewis Jr
    ATTN: L. Cohen MS 13-3
    ATTN· R. Reck
    ATTN: G. Johnson
    ATTN: E. Fitzgerald
    ATTN: H. Berkowitz
    ATTN: D. Dean

McDonnell Douglas Corp
    ATTN: M. Potter

National Academy of Sciences
    ATTN: National Materials Advisory Board
    ATTN: D. Groves

Northrop Corp
    ATTN: B. Butler
    ATTN: J. Eucs

Pacific-Sierra Research Corp
    ATTN: H. Brode, Chairman SAGE
    ATTN: G. Lang

Pan Am World Service Inc
    ATTN: AEDC/Library Doc, TRF

PDA Engineering
    ATTN: J. Schutzler
    ATTN: M. Sherman
    ATTN: J. Dunn
    ATTN: J. McDonald

Physics International Co
    ATTN: J. Shea

R&D Associates
    ATTN: W. Graham
    ATTN: P. Rausch
    ATTN: J. Carpenter
    ATTN: F. Field

Rand Corp
    ATTN: R. Rapp

Rockwell International C p
    ATTN: G. Perroue

Rockwell International Corp
    ATTN: R. Hemann

S-CUBED
    ATTN: R. Duff
    ATTN: G. Gurtman

Science Applications, Inc
    ATTN: W. Yengst
    ATTN: W. Plows
    ATTN: C. Lee
    ATTN: J. Warner
    ATTN: J. Manship
    ATTN: J. Stoddard

Science Applications, Inc
    ATTN: W. Layson
    ATTN: J. Cockayne
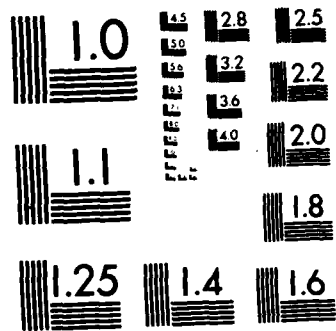
MICROCOPY RESOLUTION TEST CHART

NATIONAL BUREAU OF STANDARDS-1963-A

DEPARTMENT OF DEFENSE CONTRACTORS (Continued)

Science Applications, Inc
    ATTN: A. Martellucci

Southern Research Institute
    ATTN: C. Pears

SRI International
    ATTN: D. Curran
    ATTN: G. Abrahamson
    ATTN: H. Lindberg

System Planning Corp
    ATTN: J. Jones

Terra Tek, Inc
    ATTN: S. Green

Teledyne Brown Engrg
 4 cy ATTN: M. Price

Thiokol Corp
    ATTN: J. Hinchman
    ATTN: W. Shoun

Toyon Research Corp
    ATTN: J. Cunningham
    ATTN: B. Gragg

DEPARTMENT OF DEFENSE CONTRACTORS (Continued)

TRW Electronics & Defense Sector
    ATTN: A. Zimmerman
    ATTN: T. Williams
    ATTN: N. Lipner
    ATTN: P. Brandt
    ATTN: R. Bacharach
    ATTN: M. King
    ATTN: W. Wood
    ATTN: M. Seizew
    ATTN: R. Plebuch
    ATTN A. Ambrosio
    ATTN: D. Baer
    ATTN: T. Mazzola

TRW Electronics & Defense Sector
    ATTN: D. Kennedy
    ATTN: V. Blankinship
    ATTN: D. Glenn
    ATTN: W. Polich
    ATTN: E. Wong
    ATTN: P. Dai
    ATTN: L. Berger
    ATTN: N. Guiles
    ATTN: E. Allen

94

END

FILMED

12-83

DTIC